

THE TRANSITION FROM THE KUIPER BELT TO THE JUPITER-FAMILY COMETS

Wesley C. Fraser

Herzberg Astronomy and Astrophysics Research Centre, National Research Council,
5071 West Saanich Road, Victoria, BC, V8T 1E7, Canada
Department of Physics and Astronomy, University of Victoria, Victoria, BC, V8P 5C2, Canada

Luke Dones

Southwest Research Institute, 1050 Walnut St., Suite 300, Boulder, CO, 80504, USA

Kathryn Volk

Lunar and Planetary Laboratory, The University of Arizona, 1629 E University Blvd, Tucson, AZ, 85721
Planetary Science Institute, 1700 East Fort Lowell Rd., Suite 106, Tucson, Arizona, 85719

Maria Womack

National Science Foundation, 2415 Eisenhower Ave, Alexandria, VA 22314
Department of Physics, University of Central Florida, Orlando, FL 32816

David Nesvorný

Southwest Research Institute, 1050 Walnut St., Suite 300, Boulder, CO, 80504, USA

Kuiper Belt Objects, or more generally Trans-Neptunian Objects (TNOs), are planetesimals found beyond the orbit of Neptune. Some TNOs evolve onto Neptune-crossing orbits and become Centaurs. Many Centaurs, in turn, reach Jupiter-crossing orbits and become Jupiter-family comets (JFCs). TNOs are the main source of the JFCs. TNOs offer a different window than the JFCs, of more primordial bodies and over a different size and temperature range. It is in that context that this chapter is written. Here we discuss the dynamical pathways taken from the trans-Neptunian region to the JFCs, and the most important properties of TNOs that relate to the JFC population, including considerations of their origins, compositions, morphologies, and size distributions. We relate these properties to the JFCs whenever possible. We reflect on a few key outstanding issues regarding our incomplete knowledge of TNOs as they pertain to the Centaurs and JFC populations. We finish with a short discussion of notable new and upcoming facilities and the impacts they will have regarding these outstanding questions.

1. Introduction

Oort (1950) proposed the first, and for some time the only, reservoir for comets. He noted that, of nineteen long-period comets with well-determined orbits and semi-major axes $a \gtrsim 1,000$ au, ten had $a > 20,000$ au before they entered the planetary region. These “near-parabolic” comets had a wide range of inclinations to the ecliptic, both prograde and retrograde. Oort proposed that the solar system was surrounded by a roughly spherical cloud of $\approx 10^{11}$ comets that extended beyond $\approx 10^5$ au from the Sun, about half the distance to the nearest star.

In the wonderful words of *Kazimirchak-Polonskaya* (1972), the major planets can indeed serve as “powerful transformers of cometary orbits,” with some evolving from near-parabolic orbits onto orbits like those of Jupiter-family Comets (JFCs), which we discuss in Section 1.2 (*Everhart* 1972). However, the “capture” of Oort Cloud comets into

short-period orbits is far too inefficient to produce the observed number of JFCs (*Joss* 1973). This mismatch suggested that there must be another source of short-period comets. Several astronomers, notably *Edgeworth* (1949) and *Kuiper* (1951), suggested the existence of a belt of low-inclination comet-like bodies beyond Neptune’s orbit, ≈ 35 – 50 au from the Sun (see *Davies et al.* (2008) and *Fernández* (2020) for historical accounts of such ideas, which percolated even before the discovery of Pluto in 1930). *Fernandez* (1980) calculated that such a belt could be the source of short-period comets if it contained bodies up to the mass of Ceres ($\approx 10^{24}$ g, or 7% the mass of Pluto). *Duncan et al.* (1988) performed extensive numerical integrations and confirmed that only a low-inclination source could produce enough JFCs and proposed that this source be called the Kuiper Belt. The first Kuiper Belt Object, 15760 Albion (1992 QB₁), was discovered four years

later (Jewitt and Luu 1993).¹ Duncan et al. (1988) also remarked that Chiron, the only Centaur known at the time, “may well be a bright member of the parent population of [short-period] comets.” Hundreds of Centaurs are now known, including P/2019 LD₂ (ATLAS), an active body which passed within ≈ 0.1 au of Jupiter in 2017 and will do again in 2028 and 2063 (Steckloff et al. 2020). The 2063 encounter, the closest of the three, is expected to place the comet on an orbit with a semimajor axis $a \approx 4$ au and a perihelion distance $q < 3$ au, making it a Jupiter-family comet.

Because of the inverse-fourth-power dependence on reflected flux density with distance, the known Trans-Neptunian Objects (TNOs) are typically much larger than the Centaurs, which, in turn, are generally larger than the nuclei of JFCs. Most known TNOs have diameters of order 100 km, ranging up to Pluto and Eris (2300–2400 km); Centaurs are generally in the range of 10 to 100 km, with Chariklo the largest at 300 km; the nuclei of Jupiter-family comets range from ≈ 0.3 km up to more than 10 km. These size differences should be kept in mind when comparing different classes of bodies.

In the remainder of this section, we summarize basic orbital properties of TNOs, Centaurs, and comets, particularly the JFCs. Section 2 discusses how the Kuiper Belt attained its complex structure and the orbital evolution of TNOs to Centaurs and JFCs. In Section 3, we discuss the compositions of TNOs and Centaurs revealed by broadband colors and reflectance spectroscopy. Section 4 treats the active Centaurs, whose activity must be driven by substances more volatile than water ice; the issue of whether the frequent appearance of bilobed structures in JFCs reflects morphological evolution after leaving the Kuiper Belt or dates to the formation of these bodies billions of years ago; and the size distributions of TNOs, Centaurs, and JFCs. Section 5 concludes with a discussion of outstanding questions and future observations that may clarify many of the issues we discuss. This chapter addresses a variety of different topics regarding TNOs. Rather than providing a detailed review of a specific topic, this chapter aims to provide an overview of the most relevant TNO science relating to the field of cometary astronomy.

Many chapters in *Comets III* discuss subjects which we have no room to describe. We particularly note the chapters on the dynamical populations of comet reservoirs by Kaib and Volk; planetesimal and comet formation by Simon et al.; the chapters on cometary nuclei by Guilbert-Lepoutre et al., Pajola et al., Filacchione et al., and Knight et al.; past and future comet missions by Snodgrass et al.; and the chapter by Jewitt & Hsieh on transition objects, especially their discussion of asteroids on cometary orbits.

¹The community has referred to the objects beyond Neptune as Kuiper Belt Objects and Trans-Neptunian Objects, largely interchangeably. We adopt the latter here as a more generalized and less historically charged term.

1.1. Meet the Kuiper Belt

Three decades after the discovery of the first Trans-Neptunian Object (besides Pluto/Charon), the dynamical structure of the Kuiper Belt has proven to be more complex than that of the asteroid belt (see Gladman and Volk 2021 for a recent review). TNOs are typically classified based on 10-Myr orbital integrations, as this timescale reveals the population’s relevant key dynamical behaviors (a scheme that began with early observational surveys; e.g., Elliot et al. 2005). Gladman et al. (2008) established a widely-used classification scheme (Figure 1) that divides outer solar system objects into the following categories:

- Jupiter-coupled: Objects with semimajor axes exterior to Jupiter, but with Tisserand parameters with respect to Jupiter² less than 3.05, consistent with cometary orbits
- Centaurs: Non-Trojan objects with semimajor axes between those of Jupiter (5.2 au) and Neptune (30.1 au)
- Resonant: Objects in mean-motion resonances (MMRs) with Neptune
- Scattering: Objects whose semimajor axes vary by at least 1.5 au over 10 Myr, which typically coincides with perihelion distances $\lesssim 38$ –40 au
- Classical: Non-resonant, non-scattering objects with eccentricities < 0.24 , an arbitrary cutoff that restricts this population largely to semimajor axes between 30 and ≈ 50 au
- Detached: Objects on stable orbits that fall into none of the previous categories

The population of classical objects residing between Neptune’s 3:2 and 2:1 resonances ($39.4 < a < 47.8$ au) is often referred to as the ‘main belt’, with classical objects interior and exterior to those resonances referred to as inner and outer classical belt objects. Figure 2 shows a set of classified observed outer solar system objects that illustrates a few key dynamical features of this population: the prevalence of resonant objects, a bimodal inclination distribution extending to quite high i , and a mix of scattering and detached objects with a wide range of perihelion distances in the high- a population.

Populations of dynamically stable objects in Neptune’s MMRs were apparent from early surveys (e.g. Chiang and

²The Tisserand parameter T of a comet with respect to a planet with semimajor axis a_P is $T = a_P/a + 2 \cos i \sqrt{a(1 - e^2)/a_P}$. Here a , e , and i are the semimajor axis, eccentricity, and inclination of the comet with respect to the planet’s orbital plane. The Tisserand parameter is an approximation to the Jacobi integral, which is a constant of motion for the circular restricted three-body problem. For Jupiter-coupled comets, the Tisserand parameter varies more gradually than other orbital parameters, such as the comet’s period of revolution around the Sun (Kresák 1972; Carusi and Valsecchi 1987; Levison 1996).

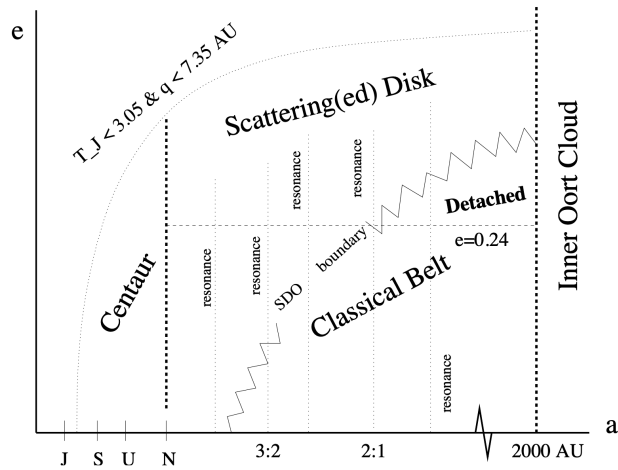


Fig. 1.— Nomenclature scheme for objects with semimajor axes beyond Jupiter’s orbit (*Gladman et al.* 2008, from). This taxonomy primarily focuses on TNOs, and, by design, excludes most JFCs. We use a similar classification.

Jordan 2002; *Elliot et al.* 2005) and predicted by early theoretical studies (e.g. *Duncan et al.* 1995; *Malhotra* 1995). Although the 3:2 MMR, which hosts Pluto and numerous “Plutinos,” contains more *known* TNOs than other resonances, the raw numbers are misleading. This is because bodies in the 3:2 have shorter orbital periods and smaller perihelion distances than most TNOs, and so are easier to discover. Analyses accounting for observational biases imply that a wide range of Neptune’s resonances in the classical belt and in more distant regions have large populations, comparable to that of the 3:2 MMR (e.g. *Gladman et al.* 2012; *Adams et al.* 2014; *Volk et al.* 2016; *Chen et al.* 2019; *Crompvoets et al.* 2022). This has important implications for the dynamical history of the outer solar system (see Section 2.1). By the late 1990s, it was clear that the orbits of observed TNOs extended to higher inclinations than did orbits of main-belt asteroids. However, there is a concentration of low-inclination orbits in the classical belt from $a = 42 - 45$ au. The bimodal nature of the inclination distribution in the classical Kuiper belt region was first demonstrated by *Brown* (2001). The low-inclination classical belt objects also tend to have low eccentricities; this sparked the division of TNO populations into categories of dynamically ‘hot’ and ‘cold’ subpopulations [meant to invoke thermodynamics because the ‘hot’ population have larger radial and vertical velocities than ‘cold’ objects] (*Levison and Stern* 2001). The cold population is essentially entirely constrained to $a = 42 - 45$ au (though with possible extensions just beyond 50 au; see, e.g., *Bannister et al.* 2018), while the scattering, detached, and the majority of the resonant populations all fall into the dynamically hot category (the implications of which are discussed in Section 2.1).

At large semimajor axes, the observed population is a

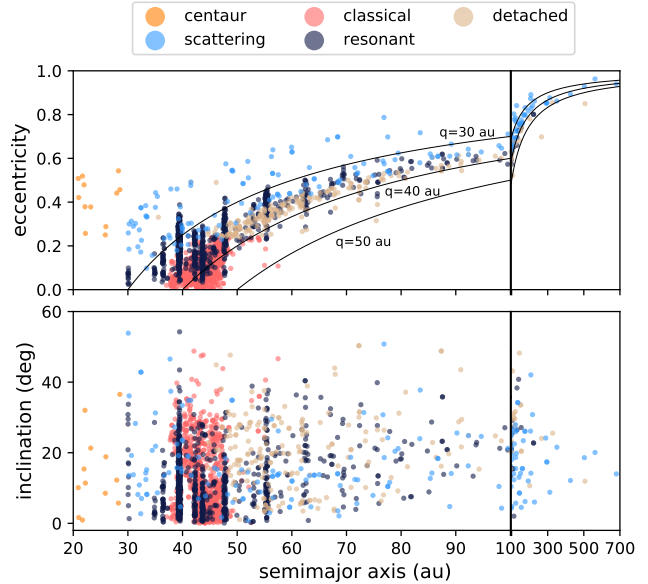


Fig. 2.— Eccentricity and inclination vs. semimajor axis of ~ 1800 observed TNOs color-coded by dynamical class; the set of TNOs is the full OSSOS sample (*Bannister et al.* 2018) combined with a subset of other TNOs in the Minor Planet Center database with classifications taken from *Smullen and Volk* (2020). The three solid lines in the top panel labeled with values between 30, 40, and 50 represent lines of constant perihelion distance. Modified from *Gladman and Volk* (2021). See Figure 8 of *Bernardinelli et al.* (2022) for a similar plot of discoveries by the Dark Energy Survey.

mix of resonant, scattering, and detached objects spanning an unexpectedly wide range of perihelion distances from 30 to 80 au. The existence of a scattered disk (*Luu et al.* 1997; *Duncan and Levison* 1997; *Volk and Malhotra* 2008) or scattering population (*Gladman et al.* 2008; *Gladman and Volk* 2021) with perihelion distances less than $\approx 37 - 40$ au is a natural consequence of objects being fed onto Neptune-crossing orbits, either today or in the early solar system (e.g., *Levison and Duncan* 1997; *Lykawka and Mukai* 2007; also see the discussion in the Kaib & Volk chapter). Objects with these smaller perihelion distances can experience perturbations from Neptune at perihelion that are strong enough to cause significant changes in orbital energy, resulting in a random walk in semimajor axis. This creates the fan-like structure in $a - e$ space seen in Figure 2, where objects are dispersed in semimajor axis along lines of constant perihelion distance (the dashed curves). Interactions with Neptune’s resonances can cause some objects’ perihelia to be raised and lowered, causing them to cycle between scattering, resonant, and detached states; other objects appear to be permanently stranded in high-perihelion detached orbits, some likely via resonant interactions during planet migration (reviewed in, e.g., *Gomes et al.* 2008). There is a subset of detached objects with such large perihelia

(90377 Sedna with $q = 76$ au, 2012 VP₁₁₃ with $q = 80$ au; *Brown et al.* 2004; *Trujillo and Sheppard* 2014; *Sheppard et al.* 2019) that they require another explanation beyond the perturbations of the giant planets (see, e.g., *Gladman and Volk* 2021). Additional large- a , large- q objects that might bridge gaps between the scattering, detached, and perhaps the inner Oort cloud populations are also beginning to be discovered (e.g., 541132 Leleakuhonua (2015 TG₃₈₇) with $q = 65$ au and $a \approx 1000$ au). As these ‘extreme’ objects do not contribute to the supply of short-period comets, we will not discuss them at length here (their implications for the solar system’s history are touched on in Section 2.1, and their possible relationship to the inner Oort cloud is discussed in the Kaib & Volk chapter).

1.2. Meet the Comets

Most comets likely formed beyond the water “snow line” ≈ 3 au from the Sun [however, the snow line’s location changes as the protoplanetary disk evolves (*Öberg et al.* 2011; *Marboeuf et al.* 2014; *Harsono et al.* 2015; *Cieza et al.* 2016; *Drozdovskaya et al.* 2016)] and within ≈ 30 au (*Nesvorný* 2018) in the solar system’s initial planetesimal disk.

Comets are commonly divided into groups based on their orbital periods. In the traditional taxonomy, long-period comets (LPCs) are defined as those with orbital periods $P > 200$ years, corresponding to $a > 34.2$ au, and short-period, or periodic, comets have $P < 200$ years. The 200-year boundary has no fundamental significance dynamically or compositionally (see, e.g. *A’Hearn et al.* 1995; *Mumma and Charnley* 2011).

Long-period comets are thought to have been gravitationally scattered by interactions with the giant planets from their closer-in formation regions ($\approx 3\text{--}30$ au) out to distances between 2,000 and $\sim 100,000$ au to form a collective known as the Oort Cloud (see, e.g. *Duncan et al.* 1987; *Vokrouhlický et al.* 2019). At those distances, perturbations external to the solar system, including passing stars and galactic tides, raise and lower comets’ perihelion distances in and out of the giant planet region and cause their orbits to take on nearly random orientations (see for example, *Weissman* 1996; *Dones et al.* 2004; also see the chapter by Kaib & Volk in this volume for further discussion of long-period comets and Oort Cloud formation).

The short-period comets can be further divided into sub-populations (*Horner et al.* 2003; *Seligman et al.* 2021). Most are classified as Jupiter-family Comets (JFCs), many of which have aphelion distances near Jupiter’s distance from the Sun (Figure 3). Most JFCs and Centaurs originate from the dynamically hot trans-Neptunian populations (Section 1.1) and orbit the Sun on prograde orbits with inclinations smaller than $\sim 30^\circ$, which is why they are also sometimes referred to as ecliptic comets, e.g., *Levison and Duncan* 1997. While most JFCs originate from the TNO populations, other populations likely contribute as well; Section 2.1 discusses this in further detail. The smaller

semimajor axes and inclinations of JFC orbits, which are not consistent with an Oort Cloud origin, pointed the way to the existence of the Kuiper belt/TNO populations prior to their discovery (e.g. *Edgeworth* 1949; *Fernandez* 1980; *Duncan et al.* 1988). This connection was later confirmed by models of the newly observed reservoir (e.g. *Levison and Duncan* 1997; *Duncan and Levison* 1997).

Historically, JFCs were often defined as comets with $P < 20$ years ($a < 7.4$ au), although a variety of definitions appear in the literature. JFCs are now often taken to be comets with Tisserand parameters with respect to Jupiter, T_J , between 2 and 3 (*Carusi and Valsecchi* 1987). This is the definition suggested by *Levison and Duncan* 1997 as being the most indicative of an origin in the Kuiper belt. Slight variations on the upper T_J limit for JFCs exist. We adopt the upper limit for JFCs of $T_J < 3.05$ from *Gladman et al.* (2008). By contrast, *Jewitt et al.* (2015) set the dividing line between Jupiter-family comets and active asteroids, some of which are main-belt comets, at $T_J = 3.08$.

Levison (1996) defined “Encke-type comets” (ETCs) as comets with $a < a_J$ and $T_J > 3$ to distinguish “decoupled” comets like 2P/Encke, whose aphelion distance is ≈ 1 au interior to Jupiter’s orbit, from typical JFCs that undergo close encounters with Jupiter. We do not find this category useful, as objects defined this way are a mix of asteroids and comets, as we discuss below. We consider Encke, which has $T_J = 3.025$, to be a JFC on an unusual orbit.

Encke’s perihelion distance $q = 0.34$ au (smaller than Mercury’s semimajor axis) is unique among comets with $T_J > 3$. Encke is generally assumed to originate in the Kuiper belt, but numerical simulations that reproduce the comet’s decoupled orbit require it to remain active for an implausibly long time (*Valsecchi et al.* 1995; *Fernández et al.* 2002; *Levison et al.* 2006b).

About half of the other “Encke-type comets” listed in the JPL Small-Body Database are active asteroids (see chapter by *Jewitt & Hsieh*). The other half are JFCs that do not cross Jupiter’s orbit, but still come within 2 Hill radii of the planet and interact strongly with it. Many of these JFCs are quasi-Hilda comets (*Tancredi et al.* 1990; *Di Sisto et al.* 2005; *Toth* 2006; *Ohtsuka et al.* 2008; *Gil-Hutton and García-Migani* 2016), which undergo slow, and thus strong encounters with Jupiter, sometimes leading to temporary captures by the planet. Indeed, D/1993 F2 (Shoemaker–Levy 9) may have been a quasi-Hilda before its capture by Jupiter and impactful demise (*Chodas and Yeomans* 1996).

Halley-type comets (HTCs) were once defined as periodic comets with orbital periods between 20 and 200 years (*Carusi et al.* 1987), but now are typically classified as periodic comets with $T_J < 2$ (e.g. *Levison and Duncan* 1994; *Levison* 1996). HTCs generally have larger semimajor axes (and higher inclinations) than the JFCs, but the new classification includes “sun-skirting” comets like 96P/Machholz with $a \approx 3$ au and perihelion distances well within the orbit of Mercury (*Jones et al.* 2018).

Halley-type comets have often been taken to be the shortest-period tail of the distribution of returning Oort

Cloud comets. However, the population of known HTC is small, about 10% that of JFCs, in large part because HTCs’ (generally) infrequent appearances provide few opportunities for discovery. The orbital distribution of Halley-type comets is therefore not very well constrained (e.g. *Wiegert and Tremaine 1999*). HTCs can be produced both from the scattering TNO population (e.g. *Brasser et al. 2012; Levison et al. 2006a*) and from the Oort Cloud (e.g. *Wang and Brasser 2014; Nesvorný et al. 2017*). More discussion of Encke- and Halley-type comets can be found in the Kaib & Volk chapter.

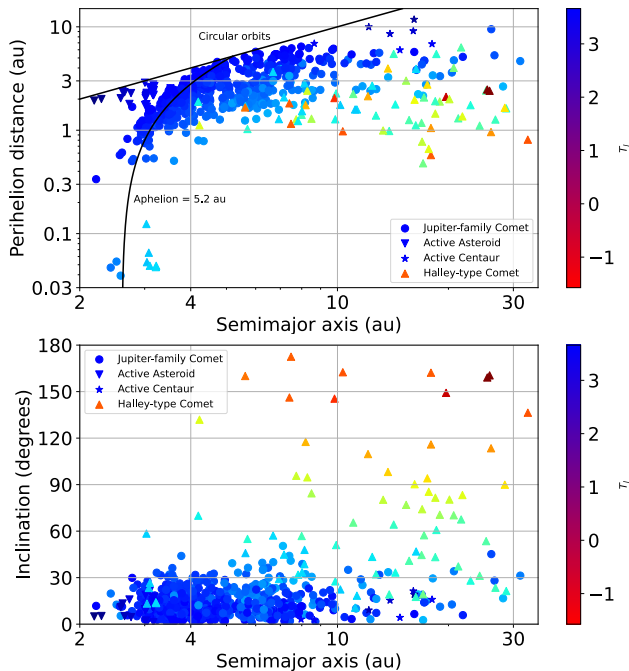


Fig. 3.— Plot of short-period comets (orbital period < 200 years, equivalent to $a \lesssim 34.2$ au) listed in the JPL Small-Body Database browser. We use the definition of *Gladman et al. (2008)* for Jupiter-family comets (JFCs), Tisserand parameter relative to Jupiter $2 < T_J < 3.05$. JFCs are denoted by circles; active asteroids ($T_J \geq 3.05$, $a < a_J$) by downward-pointing arrows; active Centaurs ($T_J \geq 3.05$, $a \geq a_J$) by stars; and Halley-type comets ($T_J \leq 2$) by upward-pointing arrows. The top panel shows perihelion distance vs. semimajor axis, while the bottom panel shows inclination vs. semimajor axis. The color scale shows T_J for each comet (right colorbars). The lines in the top panel denote circular orbits and aphelion distance equal to Jupiter’s semimajor axis of 5.2 au. Objects between the lines have orbits entirely within Jupiter’s orbit.

The population of Centaurs, small bodies with orbits in the giant planet region, provides the link between the outer solar system TNO populations and the inner solar system short-period comets. Most Centaurs are former TNOs that evolved onto Neptune-encountering orbits and were scattered inward to the giant planet region. There they have relatively short dynamical lifetimes of $\sim 1\text{--}10$ Myr (*Tis-*

careno and Malhotra 2003; Horner et al. 2004; Di Sisto and Brunini 2007; Bailey and Malhotra 2009; Fernández et al. 2018) and either evolve inward onto short-period comet orbits or outward onto highly eccentric orbits in the outer solar system; the details of this evolution are discussed in Section 2.2. Cometary activity has been detected on some Centaurs with perihelion distances as large as ≈ 12 au (e.g. *Jewitt 2009; Lilly et al. 2021*; see discussion in Section 4.1), further demonstrating that they are the transition population between the TNOs and JFCs. However, the presence of activity does not by itself show that the populations are related. For instance, although some active asteroids have sublimation-driven activity and are thus *bona fide* comets, most are thought to have resided in the asteroid belt for billions of years.

2. Origins of Trans-Neptunian Objects and Ecliptic Comets

2.1. Dynamical Origins of Trans-Neptunian Objects

How was the Kuiper Belt populated? The belt is thought to be a relic of an ancient massive planetesimal disk outside the orbits of the giant planets (*Nesvorný 2018*). *Fernandez and Ip (1984)* showed that gravitational interactions of the giant planets with small bodies cause Jupiter to lose angular momentum (because it ultimately ejects most such bodies from the solar system) and Saturn, Uranus, and Neptune to gain angular momentum. If the planetesimal disk is massive enough (comparable to Uranus or Neptune), these interactions can change the planets’ orbits substantially. *Malhotra (1993, 1995)* showed that the outward planetesimal-driven migration of Neptune would result in capture of Pluto and “Plutinos” into the 3:2 MMR. This model predicted that TNOs would also be captured into other MMRs, notably the 2:1 resonance near 48 au. TNOs in the 2:1 and many other MMRs were soon found by surveys such as DES (*Elliott et al. 2005*), CFEPS (*Petit et al. 2011*), and OSSOS (*Bannister et al. 2018*) [see Section 1.1].

In these migration scenarios, the original orbits of the giant planets would have been more closely spaced than they are now. In the Nice model (*Tsiganis et al. 2005*), Jupiter and Saturn are initially closer together then cross a mutual 2:1 resonance as a result of interactions with the planetesimal disk, exciting their eccentricities and triggering an instability in the orbits of all the giant planets (*Tsiganis et al. 2005; Levison et al. 2008; Brasser et al. 2009; Morbidelli et al. 2010; Levison et al. 2011; Nesvorný and Morbidelli 2012; Izidoro et al. 2016; Gomes et al. 2018; Quarles and Kaib 2019; Nesvorný et al. 2021*). More recent models of planetary instabilities have addressed problems with the Nice model, such as the excitation of excessively large eccentricities and inclinations in the terrestrial planets (*Brasser et al. 2009; Agnor and Lin 2012*). Efforts to match the intricate orbital distributions of the trans-Neptunian populations, asteroid belt, and other small body reservoirs have also led to substantial revision of the Nice model (see reviews by *Dones et al. 2015; Nesvorný 2018*;

Malhotra 2019; Morbidelli and Nesvorný 2020; Raymond and Nesvorný 2022). For instance, most current models invoke a fifth giant planet that was later ejected from the solar system by Jupiter (Nesvorný 2011; Nesvorný and Morbidelli 2012; Batygin et al. 2012; Cloutier et al. 2015) and find that the instability probably took place early, in the first 10–100 Myr of the solar system (Deienno et al. 2017; Mojzsis et al. 2019; De Sousa et al. 2020), rather than after hundreds of Myr (Gomes et al. 2005a). Our evolving understanding of the timing of the instability has implications for the pre-migration evolution of the disk, including the likely collisional histories of the planetesimals that eventually become the TNOs that feed the short-period comet populations (e.g. Morbidelli and Rickman 2015).

During the planetary instability, most bodies in the proto-trans-Neptunian disk are ejected from the solar system, but some reach quasi-stable niches, where they survive to the present. Models predict that the Oort Cloud and TNO populations contain the overwhelming majority of the survivors. Based on the known populations of small bodies, particularly Jupiter Trojans, and the capture efficiency found by modeling the instability, the disk is estimated to have originally contained about 6×10^9 bodies with diameters $d \gtrsim 10$ km (Morbidelli et al. 2009b; Nesvorný 2018). The instability model of Nesvorný et al. (2019b), evolved to the present, predicts the number of Centaurs of this size that OSSOS discovered to within a factor of two (also see Bottke et al. 2022). However, we know little about how many such objects reside in the TNO populations and especially the Oort Cloud. The fraction of those objects that reach the Oort Cloud and TNO populations and survive today are estimated to be $\eta = 0.05 \pm 0.01$ (Vokrouhlický et al. 2019) and 0.004 (Nesvorný et al. 2017), respectively, corresponding to $6 \times 10^9 \times 0.05 = 3 \times 10^8$ $d > 10$ km bodies in the Oort Cloud and 2×10^7 in the TNOs. Bodies from the disk are also implanted into the asteroid main belt ($\eta \approx 5 - 8 \times 10^{-6}$, Levison et al. 2009; Vokrouhlický et al. 2016), as Hildas and Trojans of Jupiter (each with $\eta \approx (6 \pm 1) \times 10^{-7}$, Nesvorný et al. 2013; Vokrouhlický et al. 2016), and as irregular satellites of Jupiter, Uranus, and Neptune (each with $\eta \approx 2 - 3 \times 10^{-8}$) and Saturn ($\eta \approx 5 \times 10^{-8}$, Nesvorný et al. 2014), yielding some 40,000 main-belt asteroids, 4,000 Hildas, 4,000 Trojans, and 100–300 irregular satellites of each giant planet.

Finding scenarios for the early evolution of the outer planets that are consistent with the complex orbital distribution of TNOs (Section 1.1) is difficult and a topic of active research. In general, some amount of planetesimal-driven migration (e.g. Fernandez and Ip 1984; Malhotra 1993, 1995) is invoked to explain the large number of resonant TNOs, while some sort of dynamical instability amongst the giant planets (e.g. Tsiganis et al. 2005) is invoked to help explain both the planets’ orbits and help dynamically excite the TNOs. Three main migration models have been proposed, which depend on the value of Neptune’s eccentricity e_N at that time: (A) very low-eccentricity ($e_N \lesssim 0.01$) migration of Neptune from

< 25 au to 30 au (e.g. Malhotra 1993, 1995; Hahn and Malhotra 2005); (B) instability-driven scattering of Neptune from < 20 au to an eccentric orbit ($e_N \sim 0.3$) at ~ 30 au, and subsequent circularization of Neptune’s orbit by dynamical friction from the planetesimal disk (e.g. Tsiganis et al. 2005; Levison et al. 2008); and (C) an intermediate case in which Neptune’s migration is interrupted by the instability, with its eccentricity reaching a peak of $e_N = 0.03$ –0.1, and then dropping to $\simeq 0.01$ as Neptune slowly migrates toward 30 au (e.g. Nesvorný and Morbidelli 2012; Nesvorný and Vokrouhlický 2016). As discussed below, these different kinds of migration models result in different distributions of the TNO populations that feed into the current comet populations.

The *original* mass and radial span of the Kuiper belt are unknown, but models that initially put several Earth masses beyond 30 au run into problems with Neptune’s migration, because Neptune continues to migrate past that distance (Gomes et al. 2004). Migration beyond 30 au can also result in excess mass in the residual belt; today’s TNOs with $r < 50$ au represent $< 0.1 M_\oplus$ (Di Ruscio et al. 2020). A sharp truncation of the original massive disk, an exponential cutoff of the disk surface density near 30 au, or some combination of the two is required to match Neptune’s orbit (Nesvorný et al. 2020). Specifically, the disk’s mass density at 30 au must have been $\lesssim 1 M_\oplus \text{au}^{-1}$ for Neptune to stop at 30 au (Nesvorný 2018). The original disk most likely continued, with a low surface density, to 45 au, where the cold classical TNOs formed and survived (Batygin et al. 2011). The current mass of cold TNOs is estimated to be only $\sim 3 \times 10^{-4} M_\oplus$ (Fraser et al. 2014) to $(3 \pm 2) \times 10^{-3} M_\oplus$ (Nesvorný et al. 2020). These values assume that TNOs have densities of 1 g cm^{-3} . The vast majority of the dynamically hot TNO populations that feed the Centaur and short period comet populations originate in the more massive, closer-in portion of this original planetesimal disk.

The three models outlined above have different implications for the hot TNO populations. A pure instability model (model B) does not explain the wide orbital inclination distribution of hot TNOs (Petit et al. 2011; Nesvorný 2015) because the instability happens so fast that there is not enough time to sufficiently excite the orbital inclinations. The existence of cold classical TNOs also limits how large Neptune’s eccentricity can be when it reaches its current semimajor axis ($e_N < 0.15$; Dawson and Murray-Clay 2012). In all three models, planetesimals originating from the < 30 au portion of the disk are scattered by Neptune to higher- a and high- e orbits; to end up in today’s metastable hot TNO populations, these orbits must subsequently be stabilized by some dynamical mechanism that causes their orbital eccentricities to drop. The Kozai resonance (Kozai 1962) near and inside mean-motion resonances with Neptune is presumably the dominant implantation mechanism during periods of slow migration (Nesvorný 2020). The Kozai resonance produces anti-correlated oscillations of e and i . As the TNO’s orbital eccentricity decreases, its orbit

can decouple from Neptune scattering (i.e., the TNO’s perihelion distance can evolve to beyond Neptune’s aphelion distance) or drop out of resonance while the TNO’s orbital inclination increases. The ν_{18} secular resonance (which occurs when a TNO’s orbital nodal precession rate matches one of the dominant nodal precession rates of the giant planets, and is the mode most associated with Neptune’s nodal rate) can also influence the inclination distribution (Volk and Malhotra 2019), but it does not wipe out the Kozai signature. When the Kozai implantation dominates for smooth migration (model A), it is difficult to obtain implanted hot TNO orbits with $i < 10^\circ$ (Figure 4). The finer details of these stabilization mechanisms and how they affect the efficiency of implantation from the original planetesimal disk into the hot TNO populations is still not fully explored, even in the simplest planetesimal driven migration scenario (model A; see discussion in Volk and Malhotra 2019).

In general, the results of migration models better match the observed hot TNO populations if Neptune’s orbit is modestly excited by an instability at some point during migration (model C). This is particularly true for matching the inclination distribution of the hot TNOs (Figure 4). In this case, bodies are implanted in the hot TNO populations as the eccentricities of high- a and high- e orbits drop due to the ν_8 secular resonance (which occurs when a TNO’s perihelion precession rate matches one of the dominant perihelion precession rates of the giant planets, the mode most associated with Neptune’s perihelion precession rate), which is stronger in this case, because $e_N \neq 0$ (Nesvorný 2021); here the contribution of Kozai cycles is relatively minor. As the ν_8 resonance does not affect inclinations, the inclination distribution is roughly preserved during implantation. The inclination distribution is then primarily controlled by Neptune’s scattering and the ν_{18} secular resonance; in some simulations, the slower Neptune’s migration is, the broader the inclination distribution becomes (Nesvorný 2015), although this is not always a generic outcome of slow migration simulations (Volk and Malhotra 2019). This model, assuming that Neptune’s migration was long-range and slow (e -folding time $\gtrsim 10$ Myr) better matches the Kuiper Belt’s orbital structure, such as its inclination distribution (Figure 4) and the fraction of TNOs in resonant orbits (Nesvorný 2018).

The scattered disk is thought to be the main source of ecliptic (or Jupiter-family) comets (Duncan and Levison 1997; Levison and Duncan 1997; Volk and Malhotra 2008; Brassier and Morbidelli 2013; Nesvorný et al. 2017) (see Section 2.2 and Dones et al. 2015 for a review of this topic). The dynamical structure of the inner detached disk (50–100 au), with dropout bodies – objects that fell out of resonance during migration on the sunward side of mean motion resonances (Bernardinelli et al. 2022) – is an important constraint on Neptune’s migration (Kaib and Sheppard 2016; Nesvorný et al. 2016; Lawler et al. 2019). The efficiency of implantation into these populations and how the inner detached disk may feed the actively scattering population on long timescales depends on the details of migration. The

scattered disk decayed by a factor of ~ 100 – 300 since its formation 4.5 Gyr ago (see, e.g., the scattered disk/Oort Cloud formation and evolution models of Brassier and Morbidelli 2013 and Nesvorný et al. (2017)). This is reflected by a rapidly decreasing number of ecliptic comets and planetary impactors soon after the instability, and a gradual decrease during the past ≈ 4 Gyr.

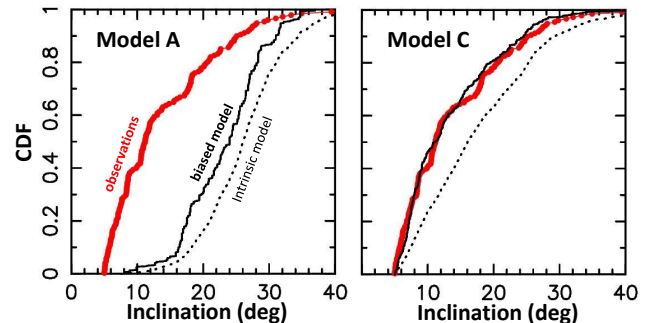


Fig. 4.— The cumulative distribution function (CDF) of TNO orbital inclinations obtained in dynamical models A (left panel) and C (right panel). The intrinsic-model, biased-model and observed distributions are shown by dotted, solid and red lines, respectively. The observed distribution shows all detections from the Outer Solar System Origins Survey (OSSOS) with $40 < a < 47$ au, $q > 36$ au and $i > 5^\circ$ (Bannister et al. 2018). The biased model distribution was obtained by applying the OSSOS survey simulator (Lawler et al. 2018a) to the intrinsic model. In model A, Neptune migrated from 24 au to 30 au with $e_N \simeq 0.01$ on a 10-Myr timescale. In model C, Neptune’s eccentricity was excited to $e_N \simeq 0.1$ when Neptune reached 28 au and slowly damped after that such that $e_N \simeq 0.01$ in the end. All planetesimals shown here started within 30 au of the Sun.

2.2. Dynamical Routes from the Centaurs to the JFCs

The short-period comets are fed into the inner solar system from the Neptune-crossing population of TNOs. This is predominantly the population of scattering objects (see discussion in the chapter by Kaib & Volk), though other subpopulations of TNOs contribute as well (see Section 2.3). Some objects on Neptune-crossing orbits will be scattered inwards into the Centaur population, from which point their evolution is dominated by gravitational scattering by the giant planets. Objects can spend upwards of ~ 100 Myr in the scattering TNO population with perihelion very near or interior to Neptune. Once an object has been transferred onto an orbit in the giant planet region, it takes ~ 1 - 10 Myr for that object to either be ejected back into the scattering population, or transferred into the JFC population (e.g. Tiscareno and Malhotra 2003; Di Sisto and Brunini 2007; Bailey and Malhotra 2009; Sarid et al. 2019; Di Sisto and Rossignoli 2020).

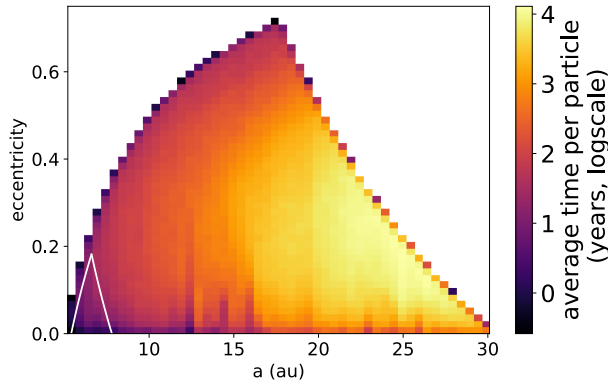


Fig. 5.— The colormap shows the time-weighted orbital distribution of Centaurs (using a definition whereby Centaurs’ orbits are entirely enclosed in the Jupiter-Neptune region) in a simulation of their evolution from the outer solar system into the JFC population (figure from *Sarid et al. 2019*).

Figure 5 illustrates the typical timespan objects spend traversing each part of the Centaur region (which in this figure from *Sarid et al. 2019* is defined as an orbit entirely enclosed between Jupiter and Neptune, $q > 5.2$ au and $Q < 30.1$ au, which is slightly more restrictive than the *Gladman et al. 2008* definition we typically use). Most of the time an object spends in the Centaur population is spent in the Uranus-Neptune region because encounters with these planets are gentler than those with Jupiter and Saturn. Even so, 20% of Centaurs will be ejected back into the outer solar system before making it inside Uranus’s orbit; only roughly half the Centaurs will be transferred onto orbits inside Saturn’s, with roughly one third making it past Jupiter to become JFCs (*Sarid et al. 2019*; see also, e.g., *Tiscareno and Malhotra 2003*; *Di Sisto and Rossignoli 2020*). Of order 1% of Centaurs will end their journeys via impact with one of the giant planets (e.g., *Levison et al. 2000*; *Tiscareno and Malhotra 2003*; *Raymond et al. 2018*; *Wong et al. 2021*). Dynamical evolution in the Centaur region is relatively insensitive to the exact source population in the outer solar system, though Centaurs with high orbital inclinations do tend to have longer lifetimes in the giant planet region due to the decreased probability of close encounters with the planets (e.g., *Di Sisto and Rossignoli 2020*). Very high inclination and retrograde Centaurs are not well-explained by the observed populations of TNOs described in Section 1.1 because the journey through the giant planet region does not radically alter the inclination distribution of Centaurs relative to their source population (e.g., *Brasser et al. 2012*; *Volk and Malhotra 2013*). The observed high-inclination Centaurs and scattering objects (e.g., *Gladman et al. 2009*; *Chen et al. 2016*) likely originate from non-TNO source regions (see discussion in the chapter by *Kaib & Volk*).

The approximately one-third of Centaurs that become JFCs (*Levison and Duncan 1997*; *Tiscareno and Malho-*

tra 2003; *Di Sisto and Brunini 2007*; *Bailey and Malhotra 2009*; *Fernández et al. 2018*) typically transfer into the inner solar system via a low-eccentricity orbit just exterior to Jupiter like that of comet 29P/Schwassmann-Wachmann 1; this orbital region, dubbed the JFC Gateway (*Sarid et al. 2019*), represents an important phase in the transition from Centaur to JFC because it coincides with thermal conditions that allow for significant cometary activity from sublimation of water ice (see, e.g., *Steckloff et al. 2020*). The Centaur to JFC transition is, of course, reversible, with objects passing back into the Centaur population (also typically through a Gateway orbit). How many JFCs survive, and in what state, to re-enter the Centaur population remains an open question.

Dynamical models of JFC orbital evolution indicate that, after becoming JFCs, it can take up to ~ 0.5 Myr for a comet to be dynamically removed (e.g., *Levison and Duncan 1994*; *Di Sisto et al. 2009*). However, during this extended orbital evolution, the JFCs’ orbital inclinations are pumped up to larger and larger values, driving the overall simulated JFC inclination distribution to disagree with the observed one (e.g., *Levison and Duncan 1994*; *Di Sisto et al. 2009*; *Nesvorný et al. 2017*). To solve this mismatch between simulated and observed JFC populations, it is usually assumed that a comet becomes inactive after some number of orbits with a perihelion distance below some threshold (often $q \lesssim 2.5$ au). Fits to the inclination distribution of JFCs with diameters between 1 and 10 km suggest physical lifetimes of ≈ 4000 – $40,000$ years (≈ 500 – 5000 orbits), which is a small fraction of the dynamical lifetimes (e.g. *Levison and Duncan 1997*; *Di Sisto et al. 2009*; *Brasser and Wang 2015*; *Nesvorný et al. 2017*). Sub-km JFC nuclei must have much shorter physical lifetimes. The exact nature of this fading (i.e., whether it is due to buildup of a surface lag layer (“mantle”, e.g. *Rickman et al. (1990)*) or physical destruction of small comet nuclei through spin-up or other mechanisms) is not well-understood; observations of dormant comet nuclei in various solar system regions (including the Centaur population) could help constrain this problem. An additional complication is that the activity of JFCs can turn on and off repeatedly. For instance, comet Blanpain (now known as 289P) was discovered in 1819, observed for two months, and not seen again for almost two centuries until it was identified with the asteroid 2003 WY25 and found to have a weak coma (*Jewitt 2006*).

2.3. Kuiper Belt Sources of Centaurs and Comets

Dynamical models of the evolution of trans-Neptunian populations confirm that the dynamically hot populations, particularly the scattering population, dominate the influx of new Centaurs and then JFCs in the inner solar system. Figure 6, for example, highlights the original orbits of particles that evolve onto cometary orbits from a model of the TNOs (*Nesvorný et al. 2017*). Most of these comet-supplying TNO orbits have perihelion distances below ~ 37 – 38 au, placing them in the scattering population, the

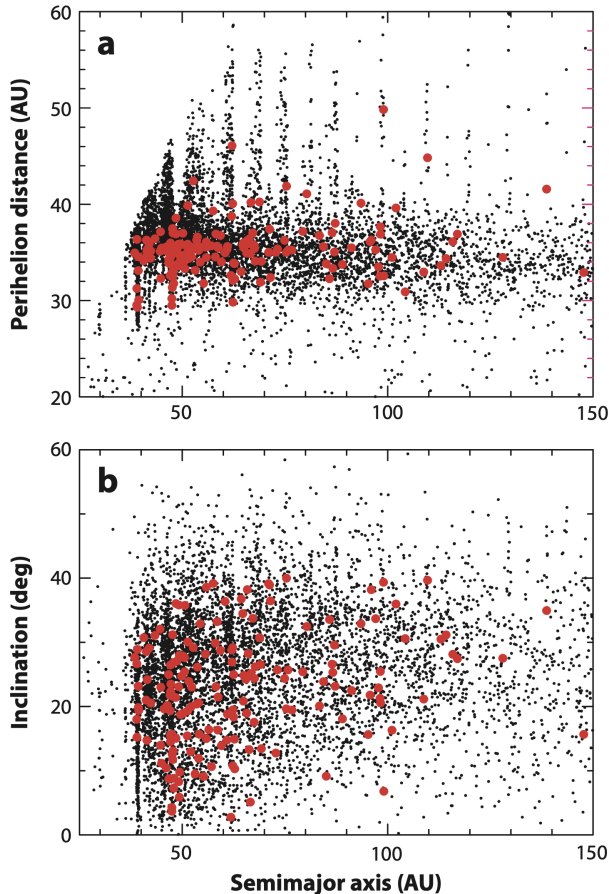


Fig. 6.— A model of the TNO population (modeled from formation to the present day) with the source-region orbits of eventual ecliptic comets highlighted. The black dots show a snapshot of the TNO population from ~ 3 Gyr ago; objects from that snapshot that later become ecliptic comets (defined as $2 < T_J < 3$, $P < 20$ years, $q < 2.5$ au) are shown as larger red dots. About 75% of TNOs that become short-period comets in this simulation originate in the scattered disk, with semimajor axes between 50 and 200 au; $\sim 20\%$ originate from TNOs with $a < 50$ au (some of which enter the 50-200 au scattering population en route); about 3% come from the Oort Cloud. From *Nesvorný* (2018), which was adapted from *Nesvorný et al.* (2017).

one originally argued to be the dominant supplier of JFCs (e.g. *Duncan and Levison* 1997). However, it is clear that a few other TNO populations also contribute to the influx. Figure 6 shows a number of JFCs sourced from Neptune’s resonant populations (vertical features most evident in the top panel). Most notable are the close-in 3:2 and 2:1 resonances, which are known to have large populations (e.g. *Volk et al.* 2016); chaotic diffusion within these resonances (and others) can slowly feed objects onto Neptune-crossing orbits that supply the JFCs (e.g. *Morbidelli* 1997; *Tiscareno and Malhotra* 2009). Figure 6 also shows a handful of high-perihelion TNO orbits that nonetheless evolve into JFCs. Most of these simulated objects appear to be in Neptune’s

more distant mean motion resonances, where secular effects cause their perihelia to cycle in and out of Neptune’s reach (e.g. *Gomes et al.* 2005b). In the real TNO population, it is still not entirely clear how many of the so-called ‘detached’ TNOs on high-perihelion orbits are still in Neptune’s resonances (and thus could cycle back into the scattering population) and how many are truly stranded at high perihelia (for example, by being dropped out of resonance during the late stages of Neptune’s migration; e.g., *Kaib and Sheppard* 2016; *Lawler et al.* 2019); this is because the orbits of very large semimajor axis TNOs are difficult to measure to high-enough precision for this determination (discussed in, e.g., *Gladman and Volk* 2021). The orbital distribution of the detached TNOs and how much that population can cycle in and out of the actively scattering population is one of the larger uncertainties in determining the exact delivery rate of JFCs from the trans-Neptunian region (also relevant to this are the effects of any unknown perturbers in the distant solar system; see discussion in *Nesvorný et al.* 2017). However, following the evolution of our best models of the TNO populations into the inner solar system (*Levison and Duncan* 1997; *Di Sisto et al.* 2009; *Brasser and Morbidelli* 2013; *Nesvorný et al.* 2017) results in an excellent match to the observed orbital distribution of comets (Figure 7), confirming that the majority of JFCs likely originate as TNOs.

For completeness, we note that a few other solar system populations may contribute to the observed JFCs. These include the low-inclination Themis family in the outer main asteroid belt (*Hsieh et al.* 2020) (also see the chapter by *Jewitt & Hsieh*), the Hildas (*Di Sisto et al.* 2005) in the 3:2 resonance with Jupiter near 4 au, and the Jupiter and Neptune Trojans (*Horner and Lykawka* 2010; *Di Sisto et al.* 2019). These sources are likely minor suppliers of the JFC population compared to the TNOs. Bodies from the primordial Kuiper Belt were implanted into all these populations (see Section 2.1), so JFCs from different present-day sources may not show clear signs of their birthplaces. Indeed, two large asteroids near the middle of the asteroid belt, 203 Pompeja and 269 Justitia, have recently been proposed to have originated as TNOs, based on their colors, which are even redder than D-type Trojans and Hildas (*Hasegawa et al.* 2021).

3. Compositions and Physical Properties

In this section, we discuss the compositions of TNOs, Centaurs, and JFCs as observed from Earth- and spacecraft-based telescopic observations. Measured properties of these objects are valuable for constraining solar system formation models (*Barucci et al.* 2011; *van der Wiel et al.* 2014). As Centaurs are thought to be an intermediate stage in the orbital evolution from TNOs to JFCs, intercomparison of their compositions can provide insights into how the journey from the scattering TNO population inward influences outgassing behavior and observed coma composition. Where available, we discuss the few compositional links between these dynamically connected populations.

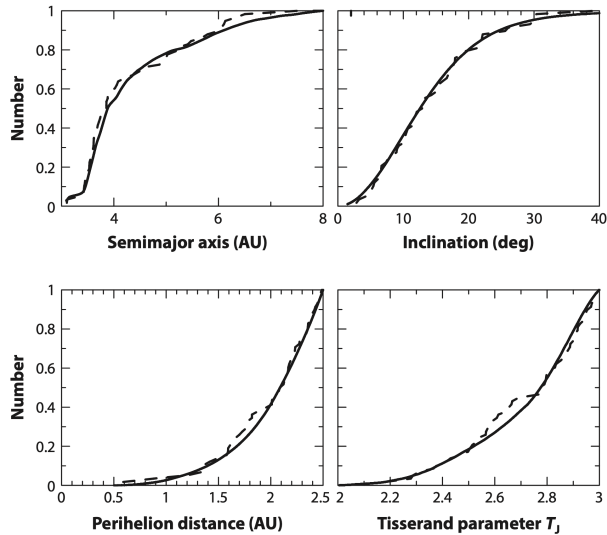


Fig. 7.— The cumulative orbital distributions of ecliptic comets with orbital periods $P < 20$ years, Tisserand parameter with respect to Jupiter $2 < T_J < 3$, and perihelion distance $q < 2.5$ au. The model results (solid lines; Nesvorný *et al.* 2017) are compared with the distribution of known JFCs (dashed lines). The model assumes that ecliptic comets remain active and visible for $N_p(2.5) = 500$ perihelion passages with $q < 2.5$ au. From Nesvorný (2018), which was adapted from Nesvorný *et al.* (2017). The panels are normalized so that the numbers of ecliptic comets with $q < 2.5$ and with $2 < T_J < 3$ equal one.

3.1. Surface Compositions of TNOs and Centaurs

Beyond atmospheric escape through processes such as Jeans loss (Lisse *et al.* 2021), TNOs are generally inactive bodies. As such, specific material identification on surfaces is made entirely through reflectance spectroscopic remote sensing. TNOs tend to have spectra that are largely devoid of identifying features (Figure 8). The detection of specific materials on the surfaces of TNOs and Centaurs is so scarce that we can easily tabulate them in Table 1, which shows the limited list of surface ices detected on these objects.

The most frequently detected material on TNOs is water ice, in both amorphous and crystalline forms (Zheng *et al.* 2009; Barucci *et al.* 2011). Water ice is thought to be abundant in all TNOs and Centaurs (Brown *et al.* 2012), and it is clearly one of the major building blocks of those bodies. Water ice absorption is most clearly seen in Haumea and its collisional family (Barkume *et al.* 2006; Trujillo *et al.* 2011). Methanol was first detected on the surface of the Centaur Pholus (Cruikshank *et al.* 1998), and has been detected with varying levels of confidence on only a handful of TNOs through ground-based spectroscopy (Barucci *et al.* 2011), and in the spectrum of Arrokoth by the New Horizon spacecraft (Grundy *et al.* 2020). Its rarity of detection implies either that its spectral signatures are usually too weak to detect, either because it is not common on TNO surfaces, or because those signatures are masked by other materials.

The former condition might imply that methanol is a by-product of some post-formation process, rather than a material that was abundant during the formation of TNOs.

The remaining materials are only found on the largest TNOs, i.e., on “dwarf planets”³, such as Eris, Pluto, Makemake, and Quaoar (for a recent summary, see Barucci and Merlin 2020). These are the known volatile ices at TNO temperatures (≈ 30 -50 K) that are unstable to sublimation on timescales shorter than the age of the solar system: N_2 , CH_4 , CO , and CO_2 . It is only by virtue of the masses of the largest TNOs that atmospheric retention of these ices is sufficient to preserve a detectable abundance of these materials since formation (Schaller and Brown 2007; Brown *et al.* 2011; Lisse *et al.* 2021). At the most basic level, the interplay between temperature and gravity governs the retention of each volatile, resulting in dramatic variations in relative abundances from object to object. This explains why some objects have spectra that are N_2 dominated (e.g. Eris), some are methane dominated (e.g. Quaoar), and some exhibit features of all the above volatile ices (e.g. Pluto). Figure 8 presents a small sample of spectra of the dwarf TNOs, exhibiting the sheer diversity of their spectra. Much like water on the Earth, the presence of these materials in a semi-stable state drives interesting atmospheric and surface re-circulation cycles that dominate the surface rheologies of these bodies (Bertrand *et al.* 2018; Hofgartner *et al.* 2019). These processes and the loss rates, which are highly sensitive to the surface and interior temperature histories of these bodies, greatly complicate estimates of the primordial ice abundances. This interesting topic is well beyond the scope of this chapter. For our purposes it is sufficient to emphasize that these volatile ices are primordial in nature, and are not fully depleted from the interiors of smaller TNOs, the interior presence of which is betrayed by the presence of these ices in the comae of JFCs (see Section 3.2).

Of course, the compositions of TNOs are not limited only to the few ices that have been spectrally identified. TNOs typically have red colors at optical wavelengths. The most striking example of this is the New Horizons flyby imagery of the small (36 km long) TNO Arrokoth (Grundy *et al.* 2020). The dynamic range of TNO/Centaur optical colors is enormous, spanning from nearly neutral reflectors (e.g. the Haumea family members; Brown *et al.* 2007) to some of the reddest objects in the solar system (e.g., Gonggong - 2007 OR10; Fraser and Brown (2012)). This red color is most commonly attributed to chemical processing of organic materials by cosmic rays (Thompson *et al.* 1987; Cruikshank *et al.* 1998; Barucci *et al.* 2011; Fraser and Brown 2012). Such materials exhibit the so-called optical gap absorption feature, driven by the C-H π -bond. Centered in the NIR, the shape and width of this feature de-

³We caution that dwarf planets should not be conflated with volatile-rich TNOs. For an object to be considered a dwarf planet requires only that it be massive enough for self-gravity to govern its shape. It is a coincidence of their formation and current surface temperatures that the dwarf-planet TNOs are the only bodies able to retain detectable levels of the volatile ices, which is the condition we are interested in here.

Table 1: Representative listing of molecules detected/inferred on surface ices and in comae or atmospheres (volatiles) of TNOs, Centaurs, and comets

| | | | | | | | | |
|----------------------|-------------------|-------------------------------|-------------------------------|-----------------------------|-------------------------------|------------------------------|-----------------------------|-------------------------------|
| TNO surface ices | H ₂ O | CH ₃ OH | CH ₄ | N ₂ | CO | CO ₂ | NH ₃ | C ₂ H ₆ |
| TNO volatiles | N ₂ | CO | CH ₄ | | | | | |
| Centaur surface ices | H ₂ O | CH ₃ OH | | | | | | |
| Centaur volatiles | CO | H ₂ O | CO ₂ | HCN | CN | CO ⁺ | N ₂ ⁺ | |
| Comet ices | H ₂ O | CO ₂ | COOH-group | | | | | |
| Comet volatiles | H ₂ O | CO ₂ | CO | CH ₄ | HCN | CH ₃ OH | H ₂ CO | NH ₃ |
| | HNC | C ₂ H ₂ | C ₂ H ₆ | HCOOH | HCOOCH ₃ | HNCO | H ₂ S | OCS |
| | HC ₃ N | SO | SO ₂ | CS | CH ₃ CO | S ₂ | CN | C ₂ |
| | NH ₂ | C ₃ | CO ⁺ | N ₂ ⁺ | H ₂ O ⁺ | CO ₂ ⁺ | N ₂ | |

pend on the amount of dehydrogenation of the organic, how disordered the molecular structure is, and the level of non-organic contaminant in the molecular chains, in particular (Seccull *et al.* 2021). This feature is common to many organic materials that are considered suitable astrophysical analogs; compare the chemically simple polycyclic aromatic hydrocarbons (e.g., Izawa *et al.* 2014) to the highly disordered laboratory materials called tholins (e.g., Roush and Dalton 2004), both of which show this deep optical gap. If attribution to organic materials is correct, the red colors of TNOs imply that simple organics such as methane were abundant for enough time in the early solar system that red dehydrogenated crusts could develop (Brunetto *et al.* 2006) before those volatile ices were depleted.

The spectrum of Arrokoth reveals a mostly featureless spectrum typical of most TNOs, except for two weak features at 1.8 and 2.2 μm . The absorption at 2.2 μm has been attributed to methanol ice (Grundy *et al.* 2020). It has been suggested that the 1.8 μm feature can be driven by the presence of sulfur in the organic residue (Mahjoub *et al.* 2021). Irradiation experiments on laboratory ice mixtures containing methane, ammonia, hydrogen sulfide, and water result in a red material bearing an absorption at 1.8 μm that is absent in mixtures with no sulfur (Mahjoub *et al.* 2021). Such a feature has not been detected on any other TNO, possibly as a result of the low available signal-to-noise ratio of even the best spectra of small TNOs. It may be that the feature is unique to the so-called cold-classical TNOs (see Section 2.1) which are the only TNO population presumed to have formed in-situ. The search for sulfur in the comae of JFCs has taken on new importance, as the presence or absence of sulfur-bearing materials in JFCs would provide significant insights regarding the compositional variations in the protoplanetary disk. The recent strong detection of atomic sulfur at 1425 Å in the JFC 46P/Wirtanen rivals that of atomic hydrogen (Noonan *et al.* 2021), and is consistent with emission directly from the nucleus or from grains very near the surface, similar to atomic sulfur and other sulfur-bearing species in 67P/Churyumov–Gerasimenko (Calmonte *et al.* 2016). Additional searches are underway for other sulfur-bearing species in JFCs to test models of cometary ices and their subsequent processing history

(Presler-Marshall *et al.* 2020; Saki *et al.* 2020; Altwegg *et al.* 2022).

No discussion about TNO compositions would be complete without the mention of silicate materials. Two TNOs, the ≈ 700 and 300-km diameter Plutinos (208996) 2003 AZ84 (Fornasier *et al.* 2009) and (120216) 2004 EW95 (Seccull *et al.* 2018), exhibit spectra that appear similar to C-type asteroids, with absorption features consistent with hydrated silicates. These two bodies are not icy, lacking even the absorptions due to water ice at 1.5 and 2.0 μm seen in the Haumea family (Brown *et al.* 1999). Frustratingly, silicate materials have avoided spectroscopic detection for icy TNOs. Their presence was first inferred by the need for silicate materials to account for the densities of the largest TNOs. Of the eleven TNOs with diameters $d > 600$ km and measured densities ρ , all but one, 55637 (2002 UX25), have $\rho > 1$ g cm⁻³ (Brown 2013; Brown and Butler 2017) [see Bierson and Nimmo (2019) and Grundy *et al.* (2019a) for densities of other TNOs]. The largest density is 2.43 ± 0.05 g cm⁻³ for Eris/Dysnomia, the most massive TNO system known (Holler *et al.* 2021). The presence of silicates has also been inferred from spectroscopic modeling, either of individual spectra (see Barucci *et al.* 2011, for example), or of the continuum of TNO optical and NIR colors (e.g. Fraser and Brown 2012). Recent modeling of spectrophotometry spanning $\sim 0.5 - 4.5$ μm implies the presence of silicate-rich surfaces amongst some of the brighter TNOs (Fernández-Valenzuela *et al.* 2021). These results demonstrate that silicates *do* exist in icy TNOs (of course they do!), but simply are masked by the presence of other materials. It is likely that characterization of silicates in TNOs will have to await observations at longer wavelengths ($\lambda \gtrsim 3$ μm ; Parker *et al.* 2016). Spectral observations from JWST are likely to be quite important in this regard (see Section 5).

Beyond spectral studies, many insights regarding the compositions of TNOs have come from broadband photometric techniques. We review those here.

Significant effort has been devoted to developing a taxonomic system for TNOs, as even the simple act of determining the number of classes is likely to influence our interpretation of the early solar system. It is generally thought

that the varied classes of TNOs reflect the compositional structure of the regions of the protoplanetary disk from which TNOs originated. Proposed mechanisms for compositional differences of planetesimals include ice lines (*Dalle Ore et al. 2015*) and post-formation volatile loss (*Wong and Brown 2016; Brown et al. 2011*), which would lead to variable composition with distance from the Sun, prior to disk dispersal by the migrating gas giants. It is important to highlight that to date, TNO compositional measurements are all measured from reflected light, and are typically assumed to be indicative of primitive nucleus values.

Efforts to determine the number of TNO classes have been frustrated by their nearly featureless spectra. TNO reflectance spectra (e.g. *Fornasier et al. 2009; Guilbert et al. 2009; Barkume et al. 2008; Barucci et al. 2011*), like those of most icy bodies, including the Jupiter Trojans, Centaurs, and JFCs (*Emery et al. 2011; Cruikshank et al. 1998; Barucci et al. 2002*) can be broadly described as linear in the optical and near-infrared (NIR), with a different spectral slope in each region, and a smooth roll-over or transition between the two slopes, very roughly centered at $\sim 0.9 \mu\text{m}$, and sometimes an absorption band of water ice at $1.5 \mu\text{m}$ and other ices in the infrared (see Sec. 3.1). A few examples are presented in Figure 8. By comparison, asteroids generally exhibit distinct features between classes that aid taxonomic interpretation (*DeMeo et al. 2009*); such features are generally unavailable for the classification of TNOs. Those few materials that have been confidently detected from the spectra of TNOs, such as water ice, do not seem to belong uniquely to certain TNO taxa. Rather, taxonomic systems have been largely generated from the variations in optical and NIR colors seen from object to object.

Centaurs and most dynamically excited TNOs exhibit a bifurcated optical color distribution (*Tegler and Romanishin 1998; Peixinho et al. 2012; Tegler et al. 2016; Fraser and Brown 2012; Peixinho et al. 2015; Lacerda et al. 2014; Marsset et al. 2019*). The bimodal color distribution has provided a functional taxonomy of two populations for small TNOs, now colloquially referred to as Red and Very Red. In this basic system, Pluto is a Red member, and Arrokoth belongs to the Very Red population of TNOs (*Grundy et al. 2020*). Intrinsically, Red class TNOs outnumber the Very Red objects by at least 4-to-1 (*Wong and Brown 2017; Schwamb et al. 2019*). This ratio has been used to infer that the purported compositional line that divides the proto-Red and proto-Very Red populations fell between 30 and 40 au (*Nesvorný et al. 2020; Buchanan et al. 2022*).

The Red/Very Red taxonomy only considers optical spectral slope or color, and does not make use of any other wavelengths. Longward of $\sim 0.9 \mu\text{m}$, TNOs tend to exhibit NIR colors that are correlated with optical spectral slope (e.g. *Fraser and Brown 2012*). Attempts have been made to use the optical-NIR color space to create more complex taxonomies. Early efforts applied principal component analysis to a sample of BVRIJ colors and found 4 classes (e.g. *Barucci et al. 2005*). This 4-taxon system

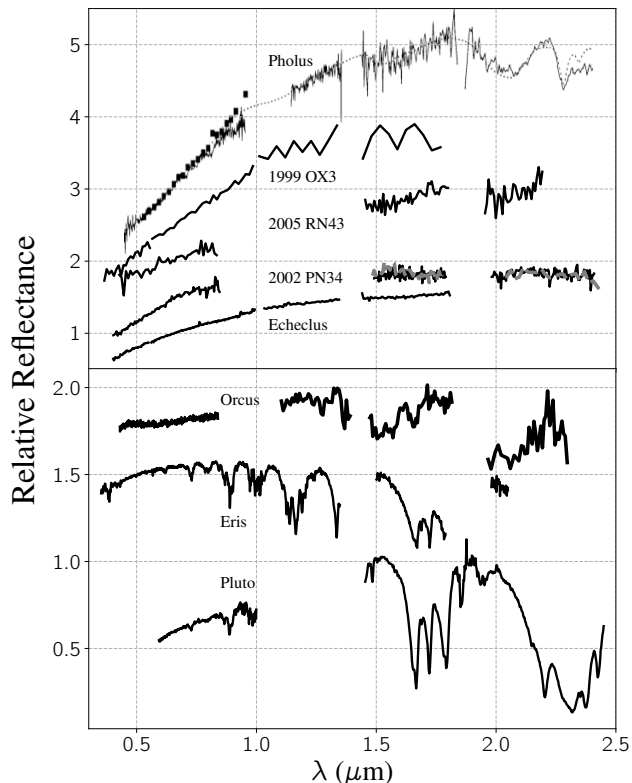


Fig. 8.— Select TNO and Centaur reflectance spectra. **Top:** spectra of (from top to bottom) the inactive Centaur 5145 Pholus (*Cruikshank et al. 1998*), TNOs (44594) 1999 OX3 (*Seccull et al. 2018*), (145452) 2005 RN43 (*Alvarez-Candal et al. 2008; Guilbert et al. 2009*), and (73480) 2002 PN34 (black *DeMeo et al. 2010*; gray *Brown et al. 2012*), and the active Centaur 60558 Echeclus, also known as comet 174P (*Seccull et al. 2018*). Spectra were normalized to unity at $0.65 \mu\text{m}$ and offset vertically in steps of 0.45. The NIR spectrum of 2005 RN43 has been renormalized to the optical spectrum using its observed (V-R) color. The dashed curve is a spectral model of Pholus, which includes contributions from olivine, tholin, water ice, and methanol. **Bottom:** Spectra of the dwarf planets Orcus (top; *DeMeo et al. 2010*), Eris (middle; *Alvarez-Candal et al. 2011*) and Pluto (bottom; *Merlin et al. 2010*). The spectra were normalized to unity at $1.5 \mu\text{m}$, and those of Orcus and Eris have been offset by 0.8 and 1.0 vertically. In both panels, regions affected by telluric lines or instrumental artifacts have been removed, and data have been rebinned for clarity. This figure omits notable objects for which the published spectra were not available to the authors, including that of the methane rich Quaoar *Jewitt (2004)*, and the water-ice rich Haumea *Trujillo et al. (2007)*.

is presented in Figure 9, and essentially divides the Red and Very Red classes into two subpopulations based on their IR behavior. For example, the IR and RR classes are Very Red, with the RR exhibiting red spectral slopes across

the BVRIJ range, and the IR exhibiting bluer NIR spectral slopes than found in the optical. Generally, the number of taxa found would increase with the number of filters or the complexity of the analysis (*Dalle Ore et al. 2013*). A recent effort to include visible albedo in the analysis expands the number of taxa to as many as 6, with an additional 4 taxa each containing a single dwarf planet (Pluto, Eris, Make-make, and Quaoar). Alternative analyses have concluded that the optical-NIR color distribution should not be further subdivided. Rather, excited TNOs exhibit only 2 separate taxa, with each exhibiting a continuum of colors through the optical and NIR color spaces (*Fraser and Brown 2012; Schwamb et al. 2019*).

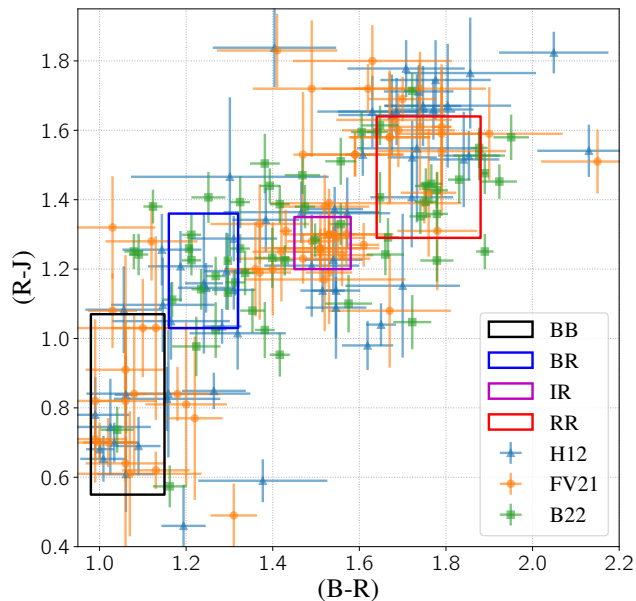


Fig. 9.— Colors of TNOs and Centaurs from *Hainaut et al. (2012, H12)*, *Fernández-Valenzuela et al. (2021, F21)*, and *Buchanan et al. (2022, B22)*. The colors of the 4-taxon system of *Barucci et al. (2005)* are shown by the rectangles *Hasegawa et al. (2021)*. Estimates of (B-R) of the *Buchanan et al. (2022)* measurements were done by determining the range of linear spectral slopes that match the reported (g-r) colors, and projecting those slopes onto (B-R). (R-J) was estimated from (r-j) in a similar fashion.

For completeness, we point out the so-called cold classical TNOs, which stand out in many ways, including their tight orbital distribution (see Section 1.1) and high binary fraction (*Noll et al. 2008, 2020*). They are found in a tight annulus between $42 < a < 48$ with inclinations $i \lesssim 5^\circ$. Considering their red optical colors (*Gulbis et al. 2006*), cold classicals mainly appear to belong to the Very Red taxon. Unlike most dynamically excited Very Red objects, however, cold classicals appear to exhibit NIR colors that tend to values closer to solar (*Pike et al. 2017*) and have higher than usual visual albedos (*Brucker et al. 2009*), suggesting cold classical objects may occupy a third taxon.

Due to their stable orbits, however, they do not act as a significant source of Centaurs or JFCs.

Unsurprisingly, the Centaurs tend to exhibit similar optical-NIR color distributions as the TNOs that feed the Centaur population. A detailed comparison is limited by biases, both observational, such as inconsistent target selection in color surveys (*Schwamb et al. 2019*), and physical, such as that colors seem to vary with size (*Benecchi et al. 2019*), and surface alteration processes (*Seccull et al. 2019*), all of which will likely affect the TNO and Centaur color distributions differently.

JFCs do not exhibit any of the color structure shown by TNOs and Centaurs. Instead, they consist entirely of objects with surfaces only slightly redder than solar (e.g. *Jewitt 2015*). As the JFCs are predominantly directly fed from the excited TNO populations, the gray surfaces of the JFCs must be the result of alterations to their surfaces as objects migrate closer to the Sun. Cometary activity seems a likely culprit. Indeed, those Centaurs which have been found to be active all have surface colors that are closer to solar than the average TNO, with none of the Centaurs with Very Red colors exhibiting detectable levels of activity. This implicates activity as a main driver for surface color alteration, possibly through deposition of gray dust (e.g. *Seccull et al. 2018*). Other alteration mechanisms might be at work, such as the thermal destruction of reddening agents.

3.2. Coma Compositions of Centaurs

At least 10–15% of known Centaurs exhibit dust comae and are deemed active (*Jewitt 2009; Bauer et al. 2013*). Such comae are composed primarily of dust grains with expansion velocities of 0.3 km s^{-1} or less and production rates ranging from $\sim 1\text{--}1,000 \text{ kg s}^{-1}$ (Table 2) (*Whitney 1955; Hughes 1991; Trigo-Rodríguez et al. 2010; Kulyk et al. 2016*). Identifying the volatile components and ascertaining which are produced in high enough amounts is an important first step in constraining models of Centaur activity and solar system formation and evolution.

A summary of volatile production rates in Centaurs is provided in Table 2. There are so few detections and significant limits that their production rates (in molecules s^{-1} and kg s^{-1}) can be listed succinctly in this table. Representative dust mass loss rates are also included in the table, with 29P leading the pack with the highest values, although low rates are sometimes seen in this Centaur.

Despite decades of observations, very few volatiles have been detected on Centaurs. This is largely due to their faintness and because most are inactive. Their distant orbits combined with only rare episodes of comae or outbursts make it difficult to discover when they are active and then carry out observations. Challenges also arise from the fact that some of the candidate species for driving activity, such as CO_2 , CH_4 , N_2 , and O_2 , are rotationally symmetric and thus have no pure rotational transitions at mm-wavelengths, which is how most cometary volatiles are observed. Furthermore, telluric contamination is a substantial obstacle for

Table 2: Measured and derived properties of dust and gas in Centaurs

| Comet | Volatile | r (au) | Production rate 10^{27} mol/s | Mass loss rate ^a (kg/s) | Reference |
|------------------------|--|-----------|------------------------------------|---------------------------------------|-----------------|
| 29P | Dust | 5.8 - 6.3 | - | 30 - 4700 | [1,2,3,4,5] |
| | CO | 5.7 - 6.3 | 10 - 70 | 460 - 3200 | [6,7,8,9,10,11] |
| | H ₂ O | 6.2-6.3 | 4.1 - 6.8 | 120 - 188 | [5, 8] |
| | CO ₂ | 6.2 | 0.5 ± 0.3 | 36 ± 22 | [12] |
| | N ₂ (N ₂ ⁺) ^b | 6.3 | 0.4 ± 0.2 | 17 ± 8 | [10, 11, 13] |
| | O ₂ ^c | 6.3 | ~0.24 | ~13 | [11] |
| | HCN | 6.3 | 0.048 ± 0.011 | 1.8 ± 0.4 | [5] |
| | CN | 5.8 | 0.008 ± 0.003 | 0.3 ± 0.1 | [14] |
| | NH ₃ | 6.3 | <4.5 | <128 | [9] |
| | CH ₃ OH | 6.3 | <0.55 | <29 | [9] |
| | CH ₄ | 6.3 | <1.3 | <34 | [9] |
| H ₂ CO | 6.3 | <0.1 | <5 | [9] | |
| Chiron | Dust | 9 - 18 | - | 1 - 45 | [15, 16, 17] |
| | CO | 8.5 | 13 ± 3 | 605 ± 151 | [18] |
| | CN | 11.3 | 0.037 ± 0.011 | 1.4 ± 0.3 | [19] |
| Echeclus | Dust | 13.1 | - | 10 - 700 | [20, 21] |
| | CO | 6.1 | 0.8 ± 0.3 | 300 ± 130 | [22] |
| | CN | 12.9 | <0.04 | < 2 | [23] |
| P/2019 LD ₂ | Dust | 4.5 | - | 40 - 60 | [24] |
| | CO | 4.58 | <4.4 | <200 | [25] |
| | CN | 4.5 | <0.0014 | < 0.1 | [23] |

[1] Fulle (1992), [2] Ivanova et al. (2011), [3] Hosek et al. (2013) [4] Schambeau et al. (2021) [5] Bockelée-Morvan et al. (2022), [6] Senay and Jewitt (1994) [7] Festou et al. (2001), [8] Ootsubo et al. (2012), [9] Paganini et al. (2013) [10] Womack et al. (2017), [11] Wierzechos and Womack (2020), [12] Harrington Pinto et al., under review, [13] Ivanova et al. (2016), [14] Cochran and Cochran (1991), [15] Luu and Jewitt (1990), [16] Romon-Martin et al. (2003), [17] Fornasier et al. (2013), [18] Womack and Stern (1999), [19] Bus et al. (1991), [20] Rousselot et al. (2016), [21] Bauer et al. (2008), [22] Wierzechos et al. (2017), [23] Rousselot (2008), [24] Licandro et al. (2021), [25] Kareta et al. (2021),

^a Gaseous mass loss rates were calculated using production rates and appropriate atomic mass units.

^b N₂ production rate is derived from CO⁺, N₂⁺ and CO measurements, see Womack et al. (2017).

^c O₂ production rate is inferred by scaling the mixing ratio of O₂ and H₂O in 67P (a JFC) to the water production rate measured in 29P by AKARI, see Wierzechos and Womack (2020) for details.

detecting CO₂ and CH₄ emission via infrared rovibrational spectra, and thus observing these two volatiles directly has been restricted to a few instruments above Earth’s atmosphere, such as the Infrared Space Observatory, AKARI Space Observatory, and in situ spacecraft mission measurements.

Highly volatile species, such as N₂ and O₂, may be abundant enough in nuclei to play a role in Centaur activity, but thus far have not been detected. N₂⁺, a probable ionization product of N₂, has been detected in optical spectra of 29P’s coma. N₂⁺ is also a frequent night sky emission feature; however, a telluric source can be ruled out with longslit spectra when N₂⁺ emission is visible only in the tailward direction (e.g., Ivanova et al. (2019)). Analysis of 29P’s N₂⁺ and CO⁺ emission in such tailward spectra of 29P is consistent with an N₂ production rate of ~ 17 kg s⁻¹, which is much smaller than CO (Wierzechos and Womack 2020). However, care should be used when interpreting either N₂⁺ and CO⁺ spectra, because their line strengths in 29P’s coma appear strongly correlated with solar wind particle veloc-

ities, possibly indicating a charging mechanism of solar-wind proton impact onto CO and N₂ in the coma (Cochran et al. 1991; Ivanova et al. 2019). An O₂ production rate was estimated by using measurements of its abundance in the Rosina mass spectroscopy of the JFC 67P, and then scaling it to the measured water production rate (Wierzechos and Womack 2020). These values suggest that N₂ and O₂ are not produced in high enough amounts to drive much of the activity of 29P.

HCN emission was detected at millimeter wavelengths in only one Centaur – 29P in 2010 – but with relatively low production rates and with a spatial profile that indicates it may have been released from icy grains and not directly sublimating from the nucleus (Bockelée-Morvan et al. 2022). Although seen in TNO and Centaur reflectance spectra, methanol (CH₃OH) emission has not yet been detected in Centaur comae, with the strongest upper limit of 29 kg s⁻¹ set for 29P (Biver 1997).

Evidence for water-ice grains has been observed in cometary comae (Yang et al. 2009; A’Hearn 2011; Kelley

et al. 2013; *Protopapa et al.* 2018); by extension, it is reasonable to search for them in Centaur comae. Centaurs orbit at heliocentric distances too large for water ice on the nucleus surface to sublimate efficiently, but water vapor may still be detected in the coma due to water ice-rich grains that are carried off the nucleus by other outgassing mechanisms and then sublimate once bathed in the solar radiation field, as was reported for 29P for water (*Ootsubo et al.* 2012) and in the aforementioned HCN. Recently, the signature of water ice grains was again reported during a significant outburst of 29P in September 2021 (*Kelley et al.* 2021), and a water ice grain signature at the 1–10% level was seen in the near-infrared spectrum of the Centaur C/2019 LD₂ (Pan-STARRS)’s coma at 4.6 au (*Kareta et al.* 2021).

There are also occasional reports of CN, C₂, and C₃ detections or upper limits. These are radicals and not capable of long-term storage in the nucleus, and so are probably daughter products from another cometary volatile and not directly responsible for driving activity (*Bus et al.* 1991; *Cochran et al.* 1991; *Womack et al.* 2017; *Ivanova et al.* 2019; *Kareta et al.* 2021; *Licandro et al.* 2021; *Bolin et al.* 2021).

Although considered as a likely candidate for distant activity in Centaurs because of its relatively high abundance in many comets and the good match of CO₂’s sublimation efficiency at Centaur distances, CO₂ emission has been searched for in Centaur comae, with no detections thus far. A significant limit was obtained only for 29P with the AKARI space telescope (*Ootsubo et al.* 2012), implying a CO/CO₂ ratio > 90, much higher than what is seen in other comets (*Harrington Pinto et al.*, under review). The space-based telescopes Spitzer and NEOWISE have been used to observe many Centaurs and were set up to detect the combined emission of CO and CO₂ in the same ~ 4.5 μm filter bandpass. Unfortunately, because the emission is combined, individual CO₂ or CO production rates cannot be derived from the data without independent and simultaneous measurements of one of the molecules. Recently, CO₂ production rates were inferred for 29P using Spitzer and NEOWISE imaging data in 2010 along with contemporaneously obtained CO millimeter-wavelength spectra, which confirms that CO₂ is produced in relatively small amounts in the 29P coma, as low as approximately 1% of CO and 14% of H₂O, (*Harrington Pinto et al.*, under review).

Consequently, CO is the most tractable volatile for direct measurement in Centaur comae that may play a significant role in activity, and these observations are possible using ground-based as well as space-based instruments at millimeter and infrared wavelengths. Detection of CO emission is reported for three Centaurs: 29P, 95P/Chiron, and 174P/Echeclus (*Senay and Jewitt* 1994; *Womack and Stern* 1999; *Wierzchos et al.* 2017; *Bockelée-Morvan et al.* 2022). On a related note, CO emission is also detected in some long-period comets at “Centaur distances” from the Sun, such as C/1995 O1 (Hale-Bopp) and C/2017 K2 (Pan-STARRS) (*Gunnarsson et al.* 2003; *Yang et al.* 2021) and CO appears to play a large role in distant comet activity

(*Biver et al.* 2002; *Womack et al.* 2017).

The apparent absence, or at least very low abundance in the coma, of CO₂ emission in 29P’s coma is instructive. If we assume that Centaurs and comets formed in similar environments and should have similar chemical compositions of their nuclei, then the available data on comets may be useful for predicting what we should see in other Centaurs. In a study of 25 comets for which CO and CO₂ were simultaneously measured, the mixing ratio of CO and CO₂ production rates showed a possible preference for CO₂ in the comae of most JFCs, but the opposite is true for some Oort Cloud comets and the lone Centaur (29P), (see *A’Hearn et al.* 2012, and *Harrington Pinto et al.*, under review) . However, if JFCs, active Centaurs, and long-period comets are analyzed as an aggregate, the coma mixing ratio may be better explained as following a heliocentric trend out to at least 6 au. CO₂ is preferentially detected in most comets (not just JFCs) within 3 au, and CO is dominant beyond 3 au, although selection effects cannot be ruled out since JFCs are typically fainter than long-period comets and less likely to be seen at large distances. However, if this trend continues for other active Centaurs, then CO emission is likely to exceed CO₂ emission in the comae of active Centaurs, as is the case for 29P. This effect may be at least partly due to differences in the degree of thermal processing of the nucleus, rather than compositional differences (*A’Hearn et al.* 2012; *Harrington Pinto and Womack* 2019). Indeed, one of the problems remaining in cometary science is accurately determining comet nucleus composition from coma abundances.

4. Activity and Physical Evolution: Comet Beginnings

4.1. Activity in Centaurs

The drivers of activity in Centaurs have implications for the nature and evolution of ice in small bodies and the cause of all activity in icy bodies at large heliocentric distances. Unfortunately, very little is known about the dominant mechanisms. Active Centaurs frequently display two types of activity: sustained comae and discrete outbursts. The first Centaur discovered, 95P/Chiron, undergoes periods of sustained activity as well as short-term brightening periods. Arguably, the best-known active Centaur is 29P, an object on a nearly circular orbit just beyond Jupiter’s distance that exhibits continuous activity with occasional outbursts of 10–250 times in brightness superimposed. Another well known active Centaur is 174P/Echeclus, which has undergone several outbursts, including a large one in which the activity was centered on an apparent fragment of the main nucleus, and a few longer-term periods of activity with lower-level dust comae.

Vigorous water-ice sublimation in comets releases many minor species in cometary comae, but Centaurs are too far from the Sun for water ice to sublimate efficiently. Thermal equilibrium temperatures of Centaur nuclei are most similar to the sublimation temperatures of CO₂ and NH₃ and hence they are favored by some models of Centaur activity, e.g.

for the Centaur C/2014 OG₃₉₂ at ~ 10 au (Chandler *et al.* 2020). However, no emission from these volatiles has yet been detected in a Centaur, and studies of 29P place stringent limits on their mixing ratio relative to CO.

As discussed in the previous section, CO is the only molecule detected in the gaseous state in active Centaurs that is capable of driving activity. CO is also abundant in a few Oort Cloud comets active beyond 5 au, but no CO detections or significant limits exist for JFCs this far out (this may not imply compositional differences between JFCs and Centaurs). There is evidence for water ice grains in the comae for two Centaurs: 29P and P/2019 LD₂ (ATLAS). These grains were most likely released from a surface component, similar to what has been reported for some Centaur and TNO surfaces in Section 3.2.

Another model for Centaur activity invokes cosmogonically important volatiles with lower sublimation temperatures, such as CO, which can survive in the nucleus as ices just below the surface, and also be partially incorporated in the gaseous state within amorphous ice and then released when this ice undergoes the phase change to the crystalline state (Priyalnik *et al.* 1995; De Sanctis *et al.* 2000; Priyalnik *et al.* 2008; Capria *et al.* 2009; Guilbert-Lepoutre 2011). This phase change is optimized around ~ 120 -140K (equivalent to Centaurs and comets at 5–10 au), but it can proceed at farther distances (and colder temperatures) less efficiently.

The most popular model that explains the observations of Centaur (and distant comet) comae is that of a nucleus with pockets of amorphous ice that undergoes the crystallization process, which releases trapped volatiles. Another model invokes isolated and insulated pockets of frozen CO or CO₂ that sublimates once the surface is disrupted enough to expose a relatively small and previously protected frozen patch (e.g. Priyalnik *et al.* 2008). However, given the very few measurements we have on Centaurs, more observations are needed to settle between these two models.

Because of the lack of detections or low production rates and significant limits for other volatiles in Centaurs, our main clues to outgassing must come from CO in 29P. The spectral line profile of CO via its J=2-1 rotational transition at 230 GHz is very narrow and slightly blueshifted, consistent with sunward emission of CO from a very cold region and a secondary source more distributed over the nucleus surface (Figure 10). This is also true for CO in Chiron (Womack and Stern 1999) and Echeclus (Wierzechos *et al.* 2017), as well as other distantly active comets like Hale-Bopp (Biver 1997; Womack *et al.* 1997) and C/2017 K2 (Pan-STARRS) (Yang *et al.* 2021). The strikingly similar spectral shapes suggest there is a common outgassing mechanism for CO in active Centaurs and distant Oort Cloud comets (Womack and Stern 1999; Biver *et al.* 2002; Gunnarsson *et al.* 2003, 2008; Wierzechos *et al.* 2017; Yang *et al.* 2021) originating from a very cold (~ 4 K) gas, (e.g., Paganini *et al.* 2013). Thus, it is reasonable to plan for narrow emission from a very cold gas in the inner coma when searching for CO in other active Centaurs.

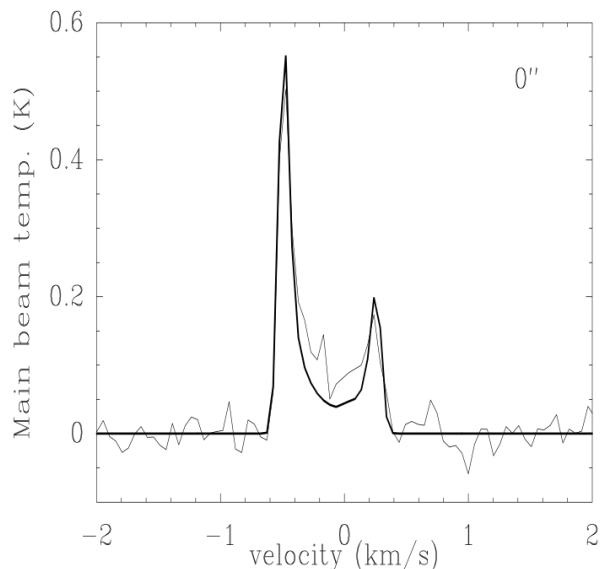


Fig. 10.— Spectral line of CO J=2-1 rotational transition at 230 GHz for the Centaur 29P/Schwassmann-Wachmann 1 obtained with the IRAM 30-m telescope in January 2004. Superimposed is a model fit to the data, which includes a strong blue-shifted peak of sunward emission from a very cold nucleus source, and a smaller contribution from the nightside. From Gunnarsson *et al.* (2008)

Interestingly, Hale-Bopp, 29P, and Echeclus appear to have approximately the same nucleus diameter and were all observed at 6 au, making an intercomparison possible that minimizes size and heliocentric distance contributions (Wierzechos *et al.* 2017). Thus, 29P is an abundant producer of CO, even sometimes outproducing Oort Cloud comet Hale-Bopp at the same distance. In contrast, Echeclus and Chiron emitted CO very weakly, and it was only marginally detected. Searches for CO in many other Centaurs did not yield detections (Drahus *et al.* 2017), but some, such as (10199) Chariklo, 342842 (2008 YB3), (8405) Asbolus, and 95626 (2002 GZ32) provide tight upper limits that eliminate the possibility of significant outgassing activity from CO at the time of observation (see Figure 11). We do not know whether Centaurs like Chiron, Echeclus, and others that produce little to no CO formed in a different environment, or whether they are devolatilized, or have not yet started to become more active, partly due to spending more of their orbits well beyond 6 au, when compared to 29P. The difference in CO output in 29P and these other active Centaurs is particularly striking and may be useful to constrain Centaur models. Further accurate measurements of nucleus diameters and CO and CO₂ production rates are needed to better understand how these species contribute to activity and ultimately to determine the composition of their nuclei.

Centaur activity also appears to be related to the resi-

CO specific production rates in Centaurs

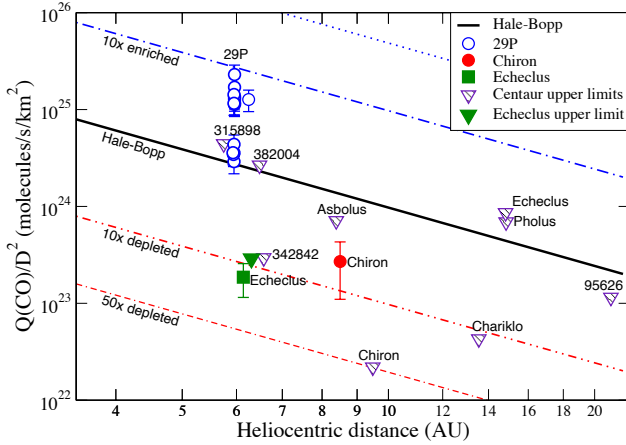


Fig. 11.— Specific gas production rates, $Q(\text{CO})/D^2$, for Centaurs. The solid line is a fit to data for Hale–Bopp provided for comparison. As the figure shows, after normalized by surface area, 29P produces far more CO than other Centaurs like Echeclus and Chiron, where CO was detected in lower amounts, and other Centaurs for which strong upper limits were set. From *Wierzchos et al. (2017)*.

dence time in its orbital region, and a decrease in perihelion distance and/or semimajor axis may occur before the observed onset of activity (*Fernández et al. 2018; Sarid et al. 2019; Lilly et al. 2021*). A Centaur’s perihelion distance also apparently plays a large role in whether a Centaur will become active, with lower values more likely to correlate with activity (*Jewitt 2009*). *Rickman et al. (1991)* noted a similar trend for short-period comets whose perihelion distances had recently decreased. Such comets had larger values for their nongravitational parameters, suggesting that their mantles had been removed, allowing more of their surfaces to be active. The ongoing CO outgassing in Centaur 29P is recently proposed to be due to the nucleus responding via the crystallization phase change of water due to the relatively sudden, within ≈ 2000 years, the median residence time of the Gateway orbit (*Sarid et al. 2019*), change in its external thermal environment produced by its dynamical migration from the Kuiper belt to the Gateway region where it maintains a nearly constant thermal environment at a heliocentric distance of ≈ 6 au (*Lisse et al. 2022*, under review). Thus, orbital history may play a large role in triggering the activity of Centaurs.

In addition to steady-state production that may produce a coma lasting weeks or months, active Centaurs sometimes have discrete outbursts lasting a few days to weeks. 29P is the best-known example whose outbursts have been documented for more than a century, primarily with secular lightcurves of the visible magnitudes and images which capture morphology in the coma, e.g., *Trigo-Rodríguez et al. (2010); Schambeau et al. (2017, 2019)*. One of the largest outbursts in decades began in September 2021, when 29P increased its brightness by a factor of ~ 250 during a

series of four smaller outbursts occurring over a few days. Such outbursts give an opportunity to test models of chemical composition and physical mechanisms of ejection. Unlike 29P, Chiron and Echeclus typically do not maintain long-term quiescent comae, but both have exhibited outbursts or brightening episodes. In 2005 Echeclus underwent a ~ 7 magnitude outburst (from 21 to 14, corresponding to an increase in brightness by a factor of ~ 630) and was accompanied by a large, detached coma ~ 2 arcmin across, projected to be 1,000,000 km at the Centaur’s distance and was visible for a few weeks (*Choi and Weissman 2006; Tegler et al. 2006; Rousselot 2008*). More details about its observational timeline, orbital dynamics and measured characteristics during outbursts are found in *Wierzchos et al. (2017); Seccull et al. (2019); Karetta et al. (2019)*.

29P’s long-term behavior of continuously having a dust and gas coma, regularly punctuated by outbursts, is well-suited to dedicated observation over years, and its lightcurve displays two types of outburst shapes: most have an asymmetric sawtooth pattern, where the reflected light grows tremendously in a few hours and then decays in days to weeks. These outbursts must have an explosive trigger that releases a great deal of dust. Less frequently, the visible lightcurves of smaller outbursts appear to grow and decay symmetrically in time (cf. *Trigo-Rodríguez et al. 2010; Wierzchos and Womack 2020; Clements and Fernandez 2021*). In contrast to the larger sawtooth shaped outbursts, the smaller symmetric outbursts may originate from a source region that spans a larger surface area on the nucleus which releases material over a longer period of time, perhaps a few days. Still another mechanism contributing to the changing brightness of Chiron is the presence of rings or ring arcs (also detected around Chariklo (*Braga-Ribas et al. 2014*)), which changes the Centaur’s apparent brightness as the aspect of the rings varies from open to edge-on (*Sickafoose et al. 2020; Fernández-Valenzuela 2022*).

There are very little data about possible triggers for the outbursts in 29P. However, outbursts of CO and dust were both recorded during simultaneous observations of CO mm-wavelength spectral flux measurements and visible magnitudes, providing an opportunity to test the hypothesis that a strong CO outburst was needed to trigger the dust outbursts. Interestingly, the CO production rate doubled, but did not trigger a noticeable rise in dust production (*Wierzchos and Womack 2020*). Similarly, two dust outbursts occurred without an accompanying increase in CO production. Two other dust outbursts may show CO gas involvement. These odd results may be explained if the CO is not always substantially incorporated with the dust component in the nucleus, or if CO is primarily released through a porous material.

4.2. Morphological Evolution and TNO Binaries in Context

The prevalence of contact binaries found in the comet and TNO populations is suggestive of a formation mecha-

nism that preferentially forms contact binary objects. Such a connection is not so obvious, however, without morphological and evolutionary considerations. This short discussion highlights only a few of the important processes one needs to consider when comparing the morphologies of JFCs to their precursor TNO populations, and the challenges faced when attempting to make inferences about their formation modes.

Most cometary nuclei imaged by spacecraft or radar have bilobed shapes; of the seven, only 9P/Tempel 1 and 81P Wild are nearly spheroidal (see the chapters by Pajola et al. and Knight et al. for further details). This suggests that comets are born bilobed or morphologically evolve to become bilobed during their lifetimes. Here we first consider the formation stage.

Formation of small planetesimals in the outer solar system favors binarity. For example, the streaming instability model (Youdin and Goodman 2005, see chapter by Simon et al.), where rotating clouds of pebbles collapse under their own gravity, gives birth to binary systems with near-equal-sized components, with properties that match observations (Grundy et al. 2019a; Nesvorný et al. 2019a). The components of a newly formed close binary can be brought into contact by gas drag (Lyra and Umurhan 2019), producing a contact binary. The early-stage low-speed collisions between similar size bodies can lead to mergers and bilobate shapes as well (Jutzi and Asphaug 2015).

Contact binaries are ubiquitous in the Kuiper Belt. For example, the New Horizons spacecraft revealed that Arrokoth is a contact binary, which likely resulted from a low-speed merger of two flattened, spheroidal components (Stern et al. 2019). Additionally, light curve observations of TNOs indicate that the contact binary fraction can be 30% or higher (Sheppard and Jewitt 2004; Thirouin and Sheppard 2018, 2019, 2022; Noll et al. 2020; Showalter et al. 2021).

It is suggestive to draw connections between these observations and bilobed comets. Note, however, that: (i) comets are much smaller than most known TNOs, and (ii) Arrokoth, with its nearly-circular, nearly-ecliptic orbit 44 au from the Sun, formed well beyond the original formation region of most comets, in a sparsely populated region of the Kuiper Belt. As discussed in Section 2.1, present-day comets presumably formed in a massive disk ~ 20 – 30 au from the Sun, became part of the scattering TNO population (at distances of ~ 50 – $1,000$ au) for ~ 4.5 Gyr, then evolved onto inner solar system orbits. The size and formation distance of TNOs affect their survival. Arrokoth is thought to be a pristine planetesimal that formed and survived essentially unchanged in the low-mass classical belt (McKinnon et al. 2020). Small comets, instead, are less likely to survive intact, their first obstacle being the disruptive and shape-changing collisions during the massive disk stage (Benavidez et al. 2022).

The overall significance of collisions during the disk stage mainly depends on the disk lifetime, t_{disk} . If $t_{\text{disk}} \gtrsim 10$ Myr, the great majority of comet-sized bodies would

be disrupted (Morbidelli and Rickman 2015), and the size distribution of small bodies would approach the Dohnanyi slope (Dohnanyi 1969; O’Brien and Greenberg 2003). This could explain the size distribution break observed near $D = 100$ km (Bernstein et al. 2004, 2006; Fraser et al. 2014, and Section 4.3). Any traces of the original surface morphology would be wiped out: most comets would be fragments of larger bodies. If $t_{\text{disk}} \ll 10$ Myr instead, 67P-sized comets would avoid being catastrophically disrupted. Smaller impacts, however, could still cause important shape changes (Jutzi and Benz 2017).

Catastrophic disruptions (Schwartz et al. 2018) and sub-catastrophic impacts on elongated and rotating bodies have been modeled to demonstrate the formation of bilobate comets (Jutzi and Benz 2017). As the massive disk was dispersed by Neptune, the collisional probabilities dropped, and the collision speeds increased from hundreds of m/s to several km/s (Nesvorný and Vokrouhlický 2019). It is likely in this situation that each catastrophic disruption was followed by sub-catastrophic impacts, and each sub-catastrophic impact – potentially capable of generating a bilobate shape – was followed by shape-changing impacts. The observed comet shapes could be a complex end product of this sequence.

As comets evolve into the inner solar system, they become affected by H_2O sublimation torques. Simulations suggest that 67P, and bilobed comets in general, should often spin up past the breakup limit, fission, and reconfiguration (Hirabayashi et al. 2016). Many new bilobate configurations can be produced by this process. CO or CO_2 sublimation-driven spin-up might be capable of disrupting a typical JFC even before it reaches the inner solar system (Safrit et al. 2021). These results highlight the important relationship between spin and morphology. Adding to that, a spinning bilobed object also better resists reconfiguration into a more spheroidal body by small impacts (Jutzi et al. 2017).

There are at least two basic possibilities: (1) small TNOs formed as contact binaries and these shapes survived, even if with some modifications, such that TNOs remained bilobed as they dynamically evolve into Centaurs/JFCs; or (2) the bilobed shapes of JFCs have nothing to do with the formation of TNOs, but instead were produced by other processes, such as impact disruption, activity (Safrit et al. 2021), rotational fission, etc., and could reflect the reaccumulation of fragments. It may be hard to distinguish between these two possibilities. One option would be to measure the shapes of a large sample of small TNOs via occultations or lightcurve surveys, and, in the long run, via spacecraft imaging. This would give us a rough sense of the fraction of contact binaries in different TNO populations, including the cold classicals. For example, option (1) could be ruled out if small cold classicals show a very low contact binary fraction. This would indicate that small planetesimals in the outer solar system did not form bilobed, therefore pointing toward evolutionary processes as the primary cause. It is worth pointing out, however, that the only small

TNO we have flown past happens to be bilobed. We could also expect some information from future surveys about the physical properties of TNO contact binaries – for example, about the relative size of individual components in each detected small contact binary – and compare that with bilobed JFCs and Centaurs. A match would be expected if small TNOs formed bilobed and the evolutionary processes have only a small effect on the overall shape.

4.3. Size Distributions of TNOs, Centaurs, and JFCs

Here we consider the size-frequency distribution (SFD) of TNOs, Centaurs, and JFCs. The SFD holds information about the formative, morphological, and destructive processes that have altered the sizes of these bodies.

The SFD of Trans-Neptunian Objects is almost always estimated from reflectance photometry of TNOs in well-characterized surveys. The cumulative distribution of apparent magnitudes m , which we will call the luminosity function (LF), is typically expressed as $\Sigma(< m) \propto 10^{\alpha m}$. Here $\Sigma(< m)$ represents the surface density in TNOs per square degree on the sky (usually on the ecliptic) of bodies with magnitudes less than (brighter than) m , and α is the slope of the distribution on a plot of $\log_{10} \Sigma$ vs. m . If the TNOs follow a power-law differential size distribution of the form $dN/dD \propto D^{-q}$, where D is the diameter of the TNO, and we assume constant albedos, then the differential SFD slope, q , and α are related by $q = 5\alpha + 1$. The cumulative size distribution is given by $N(> D) \propto D^{-\gamma}$, where $\gamma = 5\alpha = q - 1$ (e.g., Gladman et al. (2001)). Correctly converting from a magnitude distribution to an SFD relies on a number of assumptions, including (1) the albedo and size distributions are constant and do not depend on heliocentric distance, (2) shape/lightcurve effects are not important, and (3) observational biases such as the limiting magnitude of the survey are accounted for. With these limitations in mind, surveys revealed a steep LF in the outer solar system for objects brighter than $m_r \sim 25$, with slope $\alpha \sim 0.7$ or $q \sim 4.5$ (Jewitt et al. 1998; Gladman et al. 1998; Trujillo et al. 2001; Fraser et al. 2008), significantly steeper than the value of q between 3 and 4 expected for a population in steady-state collisional cascade (Dohnanyi 1969; Matthews et al. 2014; O’Brien and Greenberg 2003). Deep “pencil-beam” surveys revealed a shallower LF with slope $\alpha \sim 0.2$ at fainter magnitudes, with a transition between the bright and faint slopes at a brightness $m_R \sim 26$ (Bernstein et al. 2004, 2006; Fuentes et al. 2009; Fraser and Kavelaars 2009). This transition is referred to as the “knee” or break magnitude in the LF.

As surveys and observational techniques improved, more of the discovered objects were tracked over time, allowing accurate distance measurements and even dynamical classification of the survey discoveries. We highlight the Canada-France-Ecliptic Plane Survey, which arguably was the first survey to provide 100% tracking for all survey discoveries (Petit et al. 2011). This improvement enabled the first direct measurements of the differ-

ential absolute luminosity function (ALF), $\Sigma(H)$, where $H = m - 2.5 \log(\Delta r) - f(\alpha_p)$. Here m is the apparent magnitude of a TNO (often in R band), r and Δ are the TNO’s heliocentric and geocentric distances, α_p is the phase angle, or observer-Sun-TNO angle, in degrees, and f is a function that describes the decrease in reflectance of a TNO with increasing α_p . For the low phase angles for TNOs accessible from the Earth, f is usually linearly approximated as $f = 0.15 \alpha_p$, where α_p is measured in degrees (see Alvarez-Candal et al. 2016, for further details). The ability to measure the ALF provided higher fidelity towards inferring the true underlying SFD.

The shape of the ALF has been characterized by power-law slopes of the form $\Sigma(H) = 10^{\alpha_H(H-H_0)}$, and is known to exhibit three distinct regions. This functional form has been chosen as a matter of convenience, as it not only trivially translates to the power-law SFD discussed above, but also provides a statistically sufficient description of the observations (Fraser et al. 2014). Formative and collisional processes do not necessarily favor the production of power-law SFDs (Li et al. 2019, see chapter by Simon et al.).

The slopes of the ALF of the dynamically excited populations of TNOs are well described by

$$\alpha_H \sim \begin{cases} 0.2, & \text{for } H_r \lesssim 4 \\ 0.87, & \text{for } 4 \lesssim H_r \lesssim 8 \\ 0.2, & \text{for } H_r > 8. \end{cases} \quad (1)$$

We show a depiction of this shape in Figure 12. This ALF translates to a size distribution that is shallow for the largest TNOs ($500 \lesssim D \lesssim 2100$ km), with SFD slope $q \sim 2$ for $D \gtrsim 800$ km for a 6% albedo (Brown 2008; Fraser et al. 2014; Nesvorný et al. 2017; Abedin and Kavelaars 2022).

This part of the size distribution is colloquially referred to as the *foot* of the SFD (Fraser et al. 2012). The SFD has a steep slope $q \sim 5.25$ for objects with $100 \lesssim D \lesssim 600$ km and then becomes shallow again, with $q \sim 2$, for sizes smaller than the knee, $D \lesssim 100$ km (Fraser et al. 2014). Direct survey constraints on the SFD much below the knee (e.g., to sizes $D \ll 100$ km) are difficult to gather due to the faintness of such small objects in reflected light.

Two separate scenarios for the creation of the SFD of the hot population have been postulated. Historically, the break at $H_r \approx 8$ has been associated with the size above which catastrophic collisions rarely occur. That is, since the epoch of formation, collisions have been largely disruptive due to the high relative velocities between TNOs (e.g., Dell’Oro et al. 2013). Also, for most of the solar system’s planetesimal populations, including TNOs, smaller bodies are more numerous, and also easier to disrupt down to sub-km sizes (Benz and Asphaug 1999). The net result is that smaller bodies are more likely to be collisionally disrupted than are relatively larger bodies (Bottke et al. 2005). It follows that most of the largest bodies may have avoided disruption. The steep slope for large objects then is a result of their formation process, originally thought to occur by hierarchical accretion, and the break diameter reflects the size

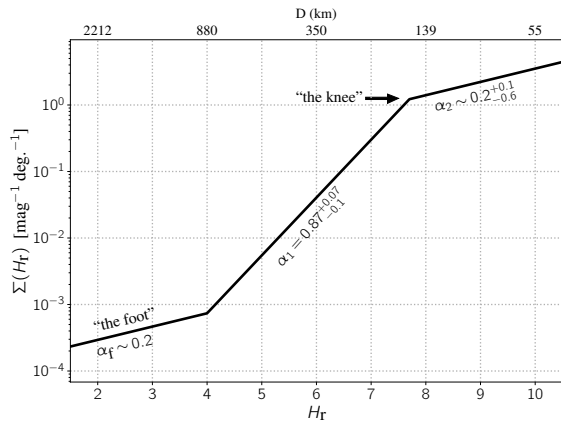


Fig. 12.— A depiction of the measured differential absolute luminosity function of the dynamically excited TNOs. Each section of the ALF is approximated by the functional form $\Sigma(H) \propto 10^{\alpha(H-H_0)}$. Slopes and transition magnitudes are taken from *Fraser et al. (2014)*. Object diameters are shown across the top, and assume a geometric albedo of 6%.

below which, on average, all objects have been collisionally disrupted. Numerical simulations bear out this idea (e.g., *Kenyon et al. 2008; Benavidez and Campo Bagatin 2009*), though recently, this interpretation has fallen out of favor. It is now thought that the observed break diameter is primordial, not collisional, in origin. If the break were collisional, the significant population of binary systems seen in the Kuiper Belt could not have survived (*Parker and Kavelaars 2010; Nesvorný and Vokrouhlický 2019*).

The alternative idea to the collisional disruption scenario is the so-called born-big scenario, first put forth to explain the size distribution of the main-belt asteroids (*Morbidelli et al. 2009a*), which has also been invoked to explain the break in the SFD of the Neptune Trojans (*Sheppard and Trujillo 2010*). In this scenario, planetesimals form with a preferred size, $D \sim 200$ km, in a formation process that is much more rapid than can be achieved through hierarchical accretion. One possible mechanism rests with the streaming instability discussed in Section 4.2. In this scenario, the break diameter reflects the preferred formation size, and the steep SFD at larger sizes reflects subsequent growth through classical hierarchical accretion. Notably, this scenario is broadly compatible with the observed properties of TNO binaries, including the frequency (*Nesvorný et al. 2011; Robinson et al. 2020*), orbital distribution (*Grundy et al. 2019b; Nesvorný 2021*), and diameters of TNOs themselves (*Li et al. 2019*).

In either scenario, the *foot* of the SFD remains unexplained. This structure seems similar to expectations from models of runaway growth (*Lithwick 2014*), though that has not been confirmed. It may also be that the foot is merely a signature of the largest objects that can form through the streaming instability.

Extension of the SFD to smaller diameters comes from

interpretation of the Pluto, Charon, and Arrokoth cratering records. At diameters $D \gtrsim 1\text{--}2$ km, the data are consistent with a slope $q \approx 3$ from the knee down to these sizes. For $D \lesssim 1\text{--}2$ km, the SFD appears to break again at the “elbow” to an even shallower slope, $q = 1.7 \pm 0.3$, betraying a relative dearth of small TNOs with $0.1 < D < 1$ km, compared with an extrapolation from larger bodies (*Greenstreet et al. 2015, 2016; Singer et al. 2019; Parker 2021; Robbins and Singer 2021; Singer et al. 2021*). A robust explanation of the change in the slope of the SFD near 1 km remains unavailable.

There is some hint of a so-called *divot* in the size distribution, just smaller than the knee diameter. The divot is a purported sudden downward deviation in the SFD, with fewer objects at sizes just below the break than above it (*Shankman et al. 2013; Lawler et al. 2018b*). Such a feature can result from a population of planetesimals that already has an SFD reminiscent of that observed (a steep slope followed by a break) that undergoes a sudden increase in velocity dispersion, such as that experienced during the onset of planet migration (*Fraser 2009*). When the velocity dispersion rises, objects suddenly have enough kinetic energy to disrupt larger bodies than those they could shatter previously. Due to the transition from a steep to shallow distribution at the break, objects larger than the break see a relative increase in disruption rate than do objects smaller than the break, with the largest relative increase occurring for bodies of size just small enough to be disrupted by objects equal to the break radius. The result is preferential destruction of bodies $\sim 10\times$ larger than the initial break radius. While the presence of a divot is not statistically required to match the observed ALF, its presence is compatible with observations, and, notably, is compatible with expectations of the formative and dynamical history of TNOs (*Fraser 2009*).

For completeness, we point out that the cold population appears to exhibit a different SFD than do the dynamically excited populations. *Fraser et al. (2014)* found that the largest cold classical objects have $D \sim 400$ km and fall on the steep part of the SFD, with a slope $q \sim 8^4$. Contrast this to the hot population SFD: the cold-classical SFD is missing the foot, and is much steeper brightward of the knee. This implies a significant difference in formation histories between those TNOs that appear to have formed in-situ, and those that were scattered outwards during Neptune’s migration. The highest fidelity measure of the cold-classical SFD (*Kavelaars et al. 2021*) demonstrates that this population is not well described by a broken power-law as in Eq. (1), but rather is better fit by a modified exponential function, $N(< H) = 10^{\alpha_S I(H-H_0)} \times \exp^{10^{\beta_S I(H-H_0)}}$, similar to the SFD produced in some simulations of formation via the streaming instability (*Li et al. 2019*). For the hot populations, it is likely that future observations will clarify

⁴In terms of absolute magnitude, the brightest cold classical TNO is 79360 Sila-Nunam (1997 CS29), which has $H = 5.29$. Sila-Nunam is a roughly equal-mass binary in which each component has $D \approx 250$ km (*Grundy et al. 2012*).

whether power laws are reasonable descriptions of the SFD of the hot population.

We also point out a tension in the populations of small, excited TNOs inferred from the ALF and the Pluto/Charon cratering record with that inferred from three serendipitous stellar occultations. Taken at face value, the occultations imply the existence of a population of small, $D \sim 1$ km excited bodies that is more than an order of magnitude larger than implied from the former techniques (Schlichting *et al.* 2012; Arimatsu *et al.* 2019; Parker 2021). A solution to this tension may be the presence of a very large population of small TNOs beyond ≈ 50 au (Shannon *et al.* 2021). It may also be the case that there is a population of small objects with extremely low albedos that have caused them to avoid optical detection. It may also be that some occultation events are not true detections, but rather are the result of unknown instrumental artifacts.

Centaurs and Jupiter-family comets provide another opportunity to probe the small-end size distribution of their parent population in the Kuiper Belt. However, there are challenges to interpreting observations of both Centaurs and JFCs. The first arises from the lack of dedicated, well-characterized surveys, particularly for Centaurs. This is primarily due to the Centaurs' small numbers, a result of their short dynamical lifetimes on planet-crossing orbits, and their wide range of ecliptic latitudes owing to their dynamically hot inclination distribution. Centaurs are thus much less dense on the sky than TNOs. Most observational surveys are focused on detecting either the close Near Earth Asteroid population or the more distant TNO populations, so the biases in the observed Centaur population are typically not well understood (see, e.g., discussion in Peixinho *et al.* 2020). Another complication is that JFCs and some Centaurs are active. For such bodies, their observed magnitudes contain contributions from (and often are dominated by) the coma, rather than just the nucleus. Astronomers have tried to minimize coma signal by taking observations when the comets are at aphelion and thus less active or inactive; however, there is always the possibility of unresolved coma that nonetheless affects the photometry (Hui and Li 2018).

With these limitations in mind, does the TNO size distribution match the JFC and Centaur size distributions? Lamy *et al.* (2004) review data on 65 ecliptic comets with effective diameters between 0.4 and 30 km, and infer a cumulative size distribution for $D \gtrsim 3$ km with $N(> D) \propto D^{-\gamma}$, where $\gamma = 1.9 \pm 0.3$, corresponding to $q \approx 2.6$ – 3.2 for the differential size distribution and $\alpha \approx 0.3$ – 0.4 for the luminosity function. Lamy *et al.* (2004) attribute the shallower size distribution seen for comets with $D \lesssim 3$ km to observational incompleteness and mass loss due to activity. Meech *et al.* (2004), on the other hand, find that the flatter slope for small comets is not explained by observational bias.

Snodgrass *et al.* (2011) performed Monte Carlo simulations of the JFC size distribution, accounting for uncertainties in photometry and the albedo, phase function, and shape of the nucleus. They inferred $\gamma = 1.92 \pm 0.20$ for nu-

clei with $D > 2.5$ km, consistent with Lamy *et al.* (2004).

The largest survey to date of Jupiter-family comets was carried out by Fernández *et al.* (2013), who observed 89 JFCs with Spitzer and included nine other JFCs from the literature. They infer $\gamma \approx 1.9 \pm 0.2$ for $D > 3$ km, but note that, surprisingly, JFCs with $D > 6$ km and $q < 2$ au are still being found. Fernández *et al.* (2013) agree with Meech *et al.* (2004) that the rarity of small comets is real.⁵ Jewitt (2021) explains the scarcity of small short-period comets as the result of sublimation torques, which he estimates can spin up comets with perihelion distances between 1 and 2 au to rotational disruption in $25(D/1 \text{ km})^2$ years, i.e., only a few orbits. The inferred SFD slopes for JFCs agree with those commonly adopted for the excited TNO parent populations, but the SFD of the Jupiter Trojans is more commonly used as a proxy for the TNO SFD for comet-sized bodies, as more Trojans are known than JFCs, and Trojans are inactive (Jewitt *et al.* 2000; Yoshida *et al.* 2019, 2020).

Using data from the Deep Ecliptic Survey, Adams *et al.* (2014) found $\alpha = 0.42 \pm 0.02$ (i.e., $\gamma = 2.1 \pm 0.1$) for seven Centaurs with absolute magnitudes between 7.5 and 11, corresponding to $30 \text{ km} \lesssim D \lesssim 170 \text{ km}$ for an assumed albedo of 0.06. OSSOS discovered 15 Centaurs with $a < 30$ au, $q > 7.5$ au, and $H_r < 13.7$ (i.e., $D > 10$ km for an albedo of 0.06). Nesvorný *et al.* (2019b) found that his planetary instability models predicted 11 ± 4 such Centaurs if he assumed $\gamma = 2.1$, similar to the slope inferred for small Trojans (Wong and Brown 2015). In general, the debiased SFDs of the JFCs and Centaurs are consistent with those measured for the TNO populations that feed the JFCs, but a detailed comparison cannot yet be made. We discuss this in Section 5.

5. Outstanding Questions and Future Prospects

In this section, we highlight three outstanding questions regarding TNOs and their link to cometary populations. We point out the anticipated contributions of certain new and upcoming telescope facilities that should provide significant leaps forward in our understanding of these questions. This list should in no way be considered impartial or complete, but rather reflects problems that the authors find particularly pertinent.

The first outstanding problem we wish to highlight regards the compositions of TNOs, and by extension the Centaurs and JFCs that are fed from the Kuiper Belt. As expressed in Section 3.1, despite more than 25 years of observations by the astronomical community, very little is known about the surfaces or internal compositions of TNOs. We are still ignorant of the nature of the reddening agent responsible for the colors of these icy bodies. Moreover, be-

⁵Since the year 2000, the number of known Near-Earth Asteroids (defined as inactive bodies with $q < 1.3$ au) has increased by a factor of ≈ 30 , while the number of Near-Earth Comets has less than doubled. These numbers are tabulated by the Center for Near Earth Object Studies at <https://cneos.jpl.nasa.gov/stats/totals.html>. Although biases in the discovery of asteroids and comets differ, the different discovery rates support the idea that small JFCs are intrinsically rare.

yond a couple of exceptions, no detection has been made of signatures of the silicate materials that must be present on and inside TNOs.

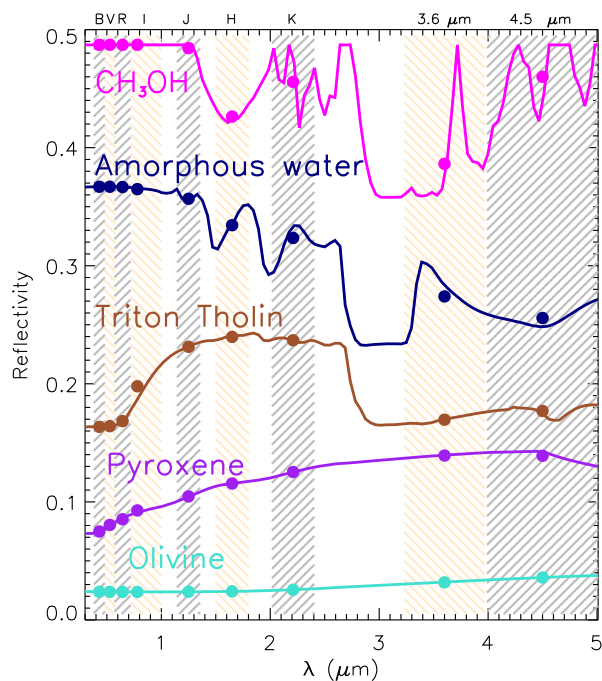


Fig. 13.— Spectra of various laboratory materials through the optical and NIR spectral range, reproduced from *Fernández-Valenzuela et al. (2021)*. Photometric bands of the Johnson-Cousins system which are accessible from ground-based facilities, as well as the Spitzer-IRAC 3.6 and 4.5 μm bands, are shown.

The main reason for this sad state of affairs is the lack of identifying absorption features in the optical and NIR atmospheric transmission regions. It seems that whatever materials are present on the surfaces of TNOs, they mutually mask any features that fall in this wavelength range. See, for example, the spectral model of the Centaur Pholus in Figure 8, where tholin and olivine mask the strong absorption features each would exhibit on their own.

Longer wavelengths hold the potential to reveal some strong absorption features. For example, many of the ice species known or suspected to exist on TNOs exhibit deep and broad absorption features in the $2.5 \lesssim \lambda \lesssim 4.5 \mu\text{m}$ range (see Figure 13). This spectral region is very difficult to observe for these faint bodies with current technology, especially ground-based because of contamination from the Earth’s atmosphere. It is for this reason that JWST holds the massive potential to revolutionize our knowledge of the compositions of TNOs.

Most insight into the compositions of TNOs will come from spectral observations with the JWST-NIRSpec instrument, which will provide unprecedented sensitivity across a critical wavelength range out to 5 μm . In Figure 14 we reproduce a figure from *Parker et al. (2016)*, which

presents three different spectral models, all of which are broadly compatible with the spectrum of the distant dwarf planet (90377) Sedna. Each model is wildly different in their compositional makeup, but are nearly indistinguishable in reflectance spectra at wavelengths $\lambda \lesssim 2.5 \mu\text{m}$. At longer wavelengths, spectra from NIRSpec will be particularly useful in diagnosing a surface as organic-rich or organic-poor, as the C-H and C-N vibrational fundamental and overtone bands fall in this range (see *Roush and Dalton 2004; Izawa et al. 2014*, for recent discussions). Ice species, including H_2O , CH_3OH , CH_4 , N_2 , CO , and CO_2 , also exhibit absorption features in this range that should be readily apparent in high-quality NIRSpec observations (see Figure 13 of this chapter, and Figure 4 of *Fernández-Valenzuela et al. 2021*).

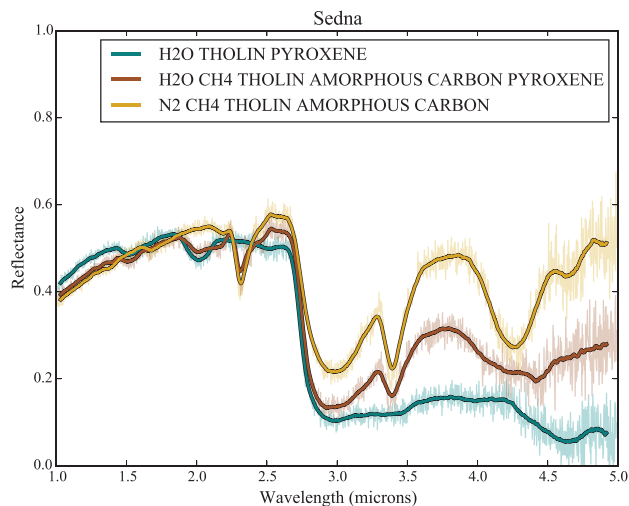


Fig. 14.— Spectral models of the TNO (90377) Sedna, using the silicate pyroxene, the organic material Titan tholin, CH_4 , and amorphous carbon, and N_2 and H_2O ices. Reproduced from *Parker et al. (2016)*.

Longer wavelength spectra in the mid-infrared range $5 < \lambda < 28 \mu\text{m}$ will come from the JWST-MIRI instrument, where fine-grained silicate materials exhibit emission features (*Martin et al. 2022*). While objects in the Kuiper Belt are too distant, and therefore too faint, for observations with MIRI, many Centaurs should be bright enough. Spitzer observed 20 Centaurs in the mid-infrared (*Lisse et al. 2020*), but obtained spectral data over the range 7.5–38 μm for only one, (8405) Asbolus (*Barucci et al. 2008*). That spectrum, which suggests the presence of fine-grained silicates on the Centaur’s surface, is broadly similar to the spectra of three Jupiter Trojans observed by Spitzer (*Dotto et al. 2008*).

Unfortunately, the low signal-to-noise of Spitzer’s spectrum of Asbolus makes it impossible to infer the nature of its putative silicates. The MIRI spectra should be of sufficient quality to not only definitively identify silicate emissions on many Centaurs, but also to identify specific properties of the silicates, such as whether those silicates are amorphous or crystalline in nature.

With regard to the volatile component, the JWST NIRSpec-IFU spectrograph is likely to either detect CO₂ emission in active Centaurs, or set strong upper limits, possibly up to two orders of magnitude less than the limit of 3.5×10^{26} for 29P achieved by AKARI (Ootsubo et al. 2012) [A. McKay, personal communication]. In addition, CO and H₂O emission will also be reachable with the instrument (see Figure 15). As discussed in Section 4.1, CO₂ is reduced with respect to CO in the comae of objects beyond 3 au, a trend that increases with heliocentric distance (Harrington Pinto et al., under review). Thus, if other Centaurs are like 29P, then their comae may be also remarkably depleted in CO₂. JWST will be capable of detecting the 1.5, 2.0 and 3.0 μm bands of water, with the 3- μm band being the one most likely to be detected in the comae of active Centaurs, and the 2- μm band being the next likely.

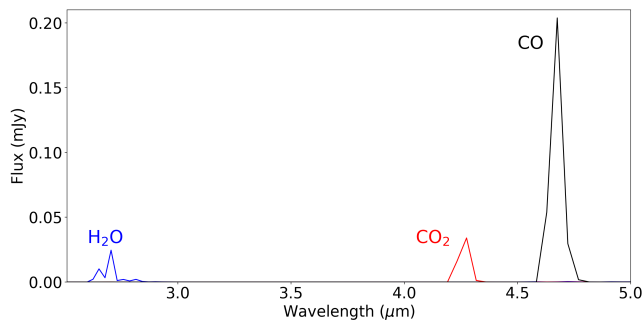


Fig. 15.— Predicted JWST NIRSpec model gas emissions for an active Centaur with a similar coma compositional profile as 29P (A. McKay, personal communication). The model was calculated using the NASA Planetary Spectrum Generator (<https://psg.gsfc.nasa.gov/> Villanueva et al. (2018)) assuming AKARI production rates for CO and H₂O from (Ootsubo et al. 2012) and inferred Q(CO₂) from Harrington Pinto et al. (under review).

An important, unanswered question about Centaur gaseous comae is whether comparing the CO, CO₂, and H₂O mixing ratios in cometary and Centaur comae is indeed a good match to compositional models of nuclei, or instead is more influenced by outgassing behavior at different heliocentric distances, due to differences in sublimation of the two species. This is a significant opportunity for the modeling community.

The second outstanding problem we wish to highlight is the discrepancy between the SFD of the JFCs and that predicted from our knowledge of the source populations feeding the JFCs (see Sections 2.1 and 2.2). While the slopes of the SFDs between the two populations seem to align (Section 4.3), there still appears disagreement between the availability of the source populations, and the observed density of JFCs. This problem was highlighted by Volk and Malhotra (2008), who found that TNOs following the Bernstein et al. (2004, 2006) SFD for faint TNOs could produce only $\approx 1\%$ of the observed JFCs. While modern models of the supply of JFCs from the TNOs match the orbital distribu-

tions of the comets well (e.g. Di Sisto et al. 2009; Brassier and Morbidelli 2013; Nesvorný et al. 2017), the problem of directly, quantitatively linking the TNO and JFC population remains frustrated by several factors: the imprecise measurement of the SFDs of the scattered disk objects and other TNO populations, especially down to comet-sized objects; the unknown ratio of active to inactive JFCs, i.e., the fading problem discussed in Section 4.3; and the incomplete knowledge of the orbital structure of the most distant TNO populations and the interplay between the scattering and detached populations (discussed in Section 2.3).

The Vera C. Rubin Telescope’s Legacy Survey of Space and Time (LSST) will provide many key insights towards resolving this problem. One of the major advances from LSST will be a much improved census of the solar system’s small bodies, down to a brightness threshold of $r \sim 24.5$, with well-understood observational biases. LSST will increase the inventory of known TNOs with well-determined orbits by at least an order of magnitude, detect large numbers of comet-sized ($d \lesssim 10$ km) Centaurs, and increase the observed JFC population (LSST Science Collaboration et al. 2009). These observations will yield important new constraints on the detailed orbital distributions of all three populations. LSST will also provide 10 years of monitoring for each discovered JFC and Centaur, on a 4–8 day cadence. This monitoring will be fundamental in detecting the onset and turnoff of activity as comets move between aphelion and perihelion, and measuring the vigor of the activity. It will also yield improved insights into the beginning stages of activity in the Centaur region. Importantly, the monitoring will enable a robust derivation of the SFD of JFCs when they are inactive, which is what is required to make a robust comparison with the Centaur and TNO populations.

A final issue is the possible presence of bodies more massive than Pluto and Eris ($0.002\text{--}0.003M_{\oplus}$) in the distant Kuiper Belt. Even with its sublunar mass, Pluto can destabilize bodies in the 3:2 MMR (Nesvorný et al. 2000). Gladman and Chan (2006) investigated how an Earth-mass body, ten Mars-mass bodies (each $\approx 0.1M_{\oplus}$), or both would raise the inclinations and perihelion distances of some objects in the primordial Kuiper Belt and produce detached bodies like Sedna. Lykawka and Mukai (2008) proposed that a planet with mass $\approx 0.5M_{\oplus}$ excited the early Kuiper Belt and evolved into a stable orbit with $a > 100$ au, $q > 80$ au, and an inclination between 20 and 40°. Trujillo and Sheppard (2014) discovered a TNO, 2012 VP₁₁₃, with $a \approx 266$ au and a perihelion distance even larger than Sedna’s, $q = 80$ au. They noted that the twelve TNOs with $a > 150$ au and $q > 30$ au appeared to cluster in argument of perihelion, and proposed that a 2–15 M_{\oplus} body could produce the clustering. This idea is now known as the “Planet Nine” hypothesis (Batygin et al. 2019; Brown and Batygin 2021) and invokes a 5–10 M_{\oplus} body with a perihelion distance ≈ 300 au to shape the orbits of TNOs with $a > 250$ au. Such a planet would even affect the orbital distributions of JFCs and HTC’s (Nesvorný et al. 2017). Well-characterized TNO surveys (Shankman et al. 2017;

Kavelaars et al. 2020; Napier et al. 2021) find that the orbital distribution of “extreme” TNOs does not require the existence of Planet Nine, but neither can it (or less massive perturbers) be ruled out. Assuming an albedo between 0.20 and 0.75, Brown and Batygin (2021) predict that Planet Nine’s most likely R magnitude is ≈ 20 , but it could be as faint as magnitude 25. Searches in the far-IR with archival IRAS and Akari data have also been carried out recently (Rowan-Robinson 2022; Sedgwick and Serjeant 2022). Observations in the next decade with the Vera Rubin Observatory and other large telescopes such as Subaru, the VLT, and Gemini should clarify the orbital distribution of distant TNOs and may finally detect the long-sSpeculated trans-Neptunian planet.

Acknowledgments

KV acknowledges support from NSF (grant AST-1824869) and NASA (grants 80NSSC19K0785, 80NSSC21K0376 and 80NSSC22K0512). LD thanks the Cassini Data Analysis Program for support. DN would like to acknowledge support from the Emerging Worlds program. This material is based in part on work done by MW while serving at the National Science Foundation. We’d especially like to thank Rosita Kokotanekova and Alan Fitzsimmons for their verbal contributions to this chapter. We thank Adam McKay and Gareth Williams for useful discussions. We also thank Sunao Hasewaga for providing data tables.

REFERENCES

Abedin A. Y. and Kavelaars J. J. (2022) in *LPI Contributions*, vol. 2678 of *LPI Contributions*, p. 1998.

Adams E. R., Gulbis A. A. S., Elliot J. L. et al. (2014) *De-biased Populations of Kuiper Belt Objects from the Deep Ecliptic Survey*, *Astron. J.*, 148, 55.

Agnor C. B. and Lin D. N. C. (2012) *On the Migration of Jupiter and Saturn: Constraints from Linear Models of Secular Resonant Coupling with the Terrestrial Planets*, *Astrophys. J.*, 745, 143.

A’Hearn M. F. (2011) *Comets as Building Blocks*, *Annu. Rev. Astron. Astrophys.*, 49, 281–299.

A’Hearn M. F., Feaga L. M., Keller H. U. et al. (2012) *Cometary Volatiles and the Origin of Comets*, *Astrophys. J.*, 758, 29.

A’Hearn M. F., Millis R. C., Schleicher D. O. et al. (1995) *The ensemble properties of comets: Results from narrowband photometry of 85 comets, 1976-1992*, *Icarus*, 118, 223–270.

Altwegg K., Combi M., Fuselier S. A. et al. (2022) *Abundant ammonium hydrosulphide embedded in cometary dust grains*, *arXiv e-prints*, arXiv:2208.11396.

Alvarez-Candal A., Fornasier S., Barucci M. A. et al. (2008) *Visible spectroscopy of the new ESO large program on trans-Neptunian objects and Centaurs. Part 1*, *Astron. Astrophys.*, 487, 741–748.

Alvarez-Candal A., Pinilla-Alonso N., Licandro J. et al. (2011) *The spectrum of (136199) Eris between 350 and 2350 nm: results with X-Shooter*, *Astron. Astrophys.*, 532, A130.

Alvarez-Candal A., Pinilla-Alonso N., Ortiz J. L. et al. (2016) *Absolute magnitudes and phase coefficients of trans-Neptunian objects*, *Astron. Astrophys.*, 586, A155.

Arimatsu K., Tsumura K., Usui F. et al. (2019) *A kilometre-sized Kuiper belt object discovered by stellar occultation using amateur telescopes*, *Nature Astronomy*, 3, 301–306.

Bailey B. L. and Malhotra R. (2009) *Two dynamical classes of Centaurs*, *Icarus*, 203, 155–163.

Bannister M. T., Gladman B. J., Kavelaars J. J. et al. (2018) *OS-SOS. VII. 800+ Trans-Neptunian Objects—The Complete Data Release*, *Astrophys. J. Suppl.*, 236, 18.

Barkume K. M., Brown M. E., and Schaller E. L. (2006) *Water Ice on the Satellite of Kuiper Belt Object 2003 EL₆₁*, *Astrophys. J. Lett.*, 640, L87–L89.

Barkume K. M., Brown M. E., and Schaller E. L. (2008) *Near-Infrared Spectra of Centaurs and Kuiper Belt Objects*, *Astron. J.*, 135, 55–67.

Barucci M. A., Alvarez-Candal A., Merlin F. et al. (2011) *New insights on ices in Centaur and Transneptunian populations*, *Icarus*, 214, 297–307.

Barucci M. A., Belskaya I. N., Fulchignoni M. et al. (2005) *Taxonomy of Centaurs and Trans-Neptunian Objects*, *Astron. J.*, 130, 1291–1298.

Barucci M. A., Brown M. E., Emery J. P. et al. (2008) in *The Solar System Beyond Neptune* (M. A. Barucci, H. Boehnhardt, D. P. Cruikshank, A. Morbidelli, and R. Dotson, eds.), pp. 143–160, Univ. of Arizona Press.

Barucci M. A., Cruikshank D. P., Mottola S. et al. (2002) in *Asteroids III* (W. F. Bottke, A. Cellino, P. Paolicchi, and R. P. Binzel, eds.), pp. 273–287, Univ. of Arizona Press.

Barucci M. A. and Merlin F. (2020) in *The Trans-Neptunian Solar System* (D. Pralnik, M. A. Barucci, and L. Young, eds.), pp. 109–126, Elsevier.

Batygin K., Adams F. C., Brown M. E. et al. (2019) *The planet nine hypothesis*, *Phys. Rep.*, 805, 1–53.

Batygin K., Brown M. E., and Betts H. (2012) *Instability-driven Dynamical Evolution Model of a Primordially Five-planet Outer Solar System*, *Astrophys. J. Lett.*, 744, L3.

Batygin K., Brown M. E., and Fraser W. C. (2011) *Retention of a Primordial Cold Classical Kuiper Belt in an Instability-Driven Model of Solar System Formation*, *Astrophys. J.*, 738, 13.

Bauer J. M., Choi Y.-J., Weissman P. R. et al. (2008) *The Large-Grained Dust Coma of 174P/Echeclus*, *PASP*, 120, 393–404.

Bauer J. M., Grav T., Blauvelt E. et al. (2013) *Centaurs and Scattered Disk Objects in the Thermal Infrared: Analysis of WISE/NEOWISE Observations*, *Astrophys. J.*, 773, 22.

Benavidez P. G. and Campo Bagatin A. (2009) *Collisional evolution of Trans-Neptunian populations: Effects of fragmentation physics and estimates of the abundances of gravitational aggregates*, *Planet. Space Sci.*, 57, 201–215.

Benavidez P. G., Campo Bagatin A., Curry J. et al. (2022) *Collisional evolution of the trans-Neptunian region in an early dynamical instability scenario*, *Mon. Not. R. Astron. Soc.*, 514, 4876–4893.

Benecchi S. D., Borncamp D., Parker A. H. et al. (2019) *The color and binarity of (486958) 2014 MU₆₉ and other long-range New Horizons Kuiper Belt targets*, *Icarus*, 334, 22–29.

Benz W. and Asphaug E. (1999) *Catastrophic Disruptions Revisited*, *Icarus*, 142, 5–20.

Bernardinelli P. H., Bernstein G. M., Sako M. et al. (2022) *A Search of the Full Six Years of the Dark Energy Survey for Outer Solar System Objects*, *Astrophys. J. Suppl.*, 258, 41.

- Bernstein G. M., Trilling D. E., Allen R. L. et al. (2004) *The Size Distribution of Trans-Neptunian Bodies*, *Astron. J.*, 128, 1364–1390.
- Bernstein G. M., Trilling D. E., Allen R. L. et al. (2006) *Erratum: The Size Distribution of Trans-Neptunian Bodies (AJ, 128, 1364 [2004])*, *Astron. J.*, 131, 2364–2364.
- Bertrand T., Forget F., Umurhan O. M. et al. (2018) *The nitrogen cycles on Pluto over seasonal and astronomical timescales*, *Icarus*, 309, 277–296.
- Biersson C. J. and Nimmo F. (2019) *Using the density of Kuiper Belt Objects to constrain their composition and formation history*, *Icarus*, 326, 10–17.
- Biver N. (1997) *Molécules mères cométaires: observations et modélisations*, Ph.D. thesis, Univ. Paris 7-Diderot.
- Biver N., Bockelée-Morvan D., Colom P. et al. (2002) *The 1995 2002 Long-Term Monitoring of Comet C/1995 O1 (HALE BOPP) at Radio Wavelength, Earth Moon and Planets*, 90, 5–14.
- Bockelée-Morvan D., Biver N., Schambeau C. A. et al. (2022) *Water, hydrogen cyanide, carbon monoxide, and dust production from distant comet 29P/Schwassmann-Wachmann 1*, *Astron. Astrophys.*, 664, A95.
- Bolin B. T., Fernandez Y. R., Lisse C. M. et al. (2021) *Initial Characterization of Active Transitioning Centaur, P/2019 LD₂ (ATLAS), Using Hubble, Spitzer, ZTF, Keck, Apache Point Observatory, and GROWTH Visible and Infrared Imaging and Spectroscopy*, *Astron. J.*, 161, 116.
- Bottke W. F., Durda D. D., Nesvorný D. et al. (2005) *Linking the collisional history of the main asteroid belt to its dynamical excitation and depletion*, *Icarus*, 179, 63–94.
- Bottke W. F., Marschall R., Vokrouhlický D. et al. (2022) in *LPI Contributions*, vol. 2678 of *LPI Contributions*, p. 2638.
- Braga-Ribas F., Sicardy B., Ortiz J. L. et al. (2014) *A ring system detected around the Centaur (10199) Chariklo*, *Nature*, 508, 72–75.
- Brasser R. and Morbidelli A. (2013) *Oort cloud and Scattered Disc formation during a late dynamical instability in the Solar System*, *Icarus*, 225, 40–49.
- Brasser R., Morbidelli A., Gomes R. et al. (2009) *Constructing the secular architecture of the solar system II: the terrestrial planets*, *Astron. Astrophys.*, 507, 1053–1065.
- Brasser R., Schwamb M. E., Lykawka P. S. et al. (2012) *An Oort cloud origin for the high-inclination, high-perihelion Centaurs*, *Mon. Not. R. Astron. Soc.*, 420, 3396–3402.
- Brasser R. and Wang J. H. (2015) *An updated estimate of the number of Jupiter-family comets using a simple fading law*, *Astron. Astrophys.*, 573, A102.
- Brown M. E. (2001) *The Inclination Distribution of the Kuiper Belt*, *Astron. J.*, 121, 2804–2814.
- Brown M. E. (2008) in *The Solar System Beyond Neptune* (M. A. Barucci, H. Boehnhardt, D. P. Cruikshank, A. Morbidelli, and R. Dotson, eds.), pp. 335–334, Univ. of Arizona Press.
- Brown M. E. (2013) *The Density of Mid-sized Kuiper Belt Object 2002 UX25 and the Formation of the Dwarf Planets*, *Astrophys. J. Lett.*, 778, L34.
- Brown M. E., Barkume K. M., Ragozzine D. et al. (2007) *A collisional family of icy objects in the Kuiper belt*, *Nature*, 446, 294–296.
- Brown M. E. and Batygin K. (2021) *The Orbit of Planet Nine*, *Astron. J.*, 162, 219.
- Brown M. E. and Butler B. J. (2017) *The Density of Mid-sized Kuiper Belt Objects from ALMA Thermal Observations*, *Astron. J.*, 154, 19.
- Brown M. E., Schaller E. L., and Fraser W. C. (2011) *A Hypothesis for the Color Diversity of the Kuiper Belt*, *Astrophys. J. Lett.*, 739, L60.
- Brown M. E., Schaller E. L., and Fraser W. C. (2012) *Water Ice in the Kuiper Belt*, *Astron. J.*, 143, 146.
- Brown M. E., Trujillo C., and Rabinowitz D. (2004) *Discovery of a Candidate Inner Oort Cloud Planetoid*, *Astrophys. J.*, 617, 645–649.
- Brown R. H., Cruikshank D. P., and Pendleton Y. (1999) *Water Ice on Kuiper Belt Object 1996 TO₆₆*, *Astrophys. J. Lett.*, 519, L101–L104.
- Brucker M. J., Grundy W. M., Stansberry J. A. et al. (2009) *High albedos of low inclination Classical Kuiper belt objects*, *Icarus*, 201, 284–294.
- Brunetto R., Barucci M. A., Dotto E. et al. (2006) *Ion Irradiation of Frozen Methanol, Methane, and Benzene: Linking to the Colors of Centaurs and Trans-Neptunian Objects*, *Astrophys. J.*, 644, 646–650.
- Buchanan L. E., Schwamb M. E., Fraser W. C. et al. (2022) *Col-OSSOS: Probing Ice Line/Color Transitions within the Kuiper Belt's Progenitor Populations*, *Planetary Sci. J.*, 3, 9.
- Bus S. J., A'Hearn M. F., Schleicher D. G. et al. (1991) *Detection of CN Emission from (2060) Chiron*, *Science*, 251, 774–777.
- Calmonte U., Altwegg K., Balsiger H. et al. (2016) *Sulphur-bearing species in the coma of comet 67P/Churyumov-Gerasimenko*, *Mon. Not. R. Astron. Soc.*, 462, S253–S273.
- Capria M. T., Coradini A., de Sanctis M. C. et al. (2009) *Thermal modeling of the active Centaur P/2004 A1 (LONEOS)*, *Astron. Astrophys.*, 504, 249–258.
- Carusi A., Kresak L., Perozzi E. et al. (1987) *High-Order Librations of Halley-Type Comets*, *Astron. Astrophys.*, 187, 899.
- Carusi A. and Valsecchi G. B. (1987) *Dynamical evolution of short-period comets*, *Publications of the Astronomical Institute of the Czechoslovak Academy of Sciences*, 2, 21–28.
- Chandler C. O., Kueny J. K., Trujillo C. A. et al. (2020) *Cometary Activity Discovered on a Distant Centaur: A Nonaqueous Sublimation Mechanism*, *Astrophys. J. Lett.*, 892, L38.
- Chen Y.-T., Gladman B., Volk K. et al. (2019) *OSSOS XVIII. Constraining Migration Models with the 2:1 Resonance Using the Outer Solar System Origins Survey*, *Astron. J.*, 158, 214.
- Chen Y.-T., Lin H. W., Holman M. J. et al. (2016) *Discovery of a New Retrograde Trans-Neptunian Object: Hint of a Common Orbital Plane for Low Semimajor Axis, High-inclination TNOs and Centaurs*, *Astrophys. J. Lett.*, 827, L24.
- Chiang E. I. and Jordan A. B. (2002) *On the Plutinos and Twotinos of the Kuiper Belt*, *Astron. J.*, 124, 3430–3444.
- Chodas P. W. and Yeomans D. K. (1996) in *IAU Colloq. 156: The Collision of Comet Shoemaker-Levy 9 and Jupiter* (K. S. Noll, H. A. Weaver, and P. D. Feldman, eds.), pp. 1–30, Cambridge University Press.
- Choi Y.-J. and Weissman P. (2006) in *AAS/Division for Planetary Sciences Meeting Abstracts #38*, vol. 38 of *AAS/Division for Planetary Sciences Meeting Abstracts*, p. 37.05.
- Cieza L. A., Casassus S., Tobin J. et al. (2016) *Imaging the water snow-line during a protostellar outburst*, *Nature*, 535, 258–261.
- Clements T. D. and Fernandez Y. (2021) *Dust Production from Mini Outbursts of Comet 29P/Schwassmann-Wachmann 1*, *Astron. J.*, 161, 73.
- Cloutier R., Tamayo D., and Valencia D. (2015) *Could Jupiter or Saturn Have Ejected a Fifth Giant Planet?*, *Astrophys. J.*, 813,

8.

- Cochran A. L. and Cochran W. D. (1991) *The first detection of CN and the distribution of CO⁺ gas in the coma of Comet P/Schwassmann-Wachmann 1*, *Icarus*, 90, 172–175.
- Cochran A. L., Cochran W. D., Barker E. S. et al. (1991) *The development of the CO⁺ coma of Comet P/Schwassmann-Wachmann 1*, *Icarus*, 92, 179–183.
- Crompvoets B. L., Lawler S. M., Volk K. et al. (2022) *OSSOS XXV: Large Populations and Scattering-Sticking in the Distant Trans-Neptunian Resonances*, *Planetary Sci. J.*, 3, 113.
- Cruikshank D. P., Roush T. L., Bartholomew M. J. et al. (1998) *The Composition of Centaur 5145 Pholus*, *Icarus*, 135, 389–407.
- Dalle Ore C. M., Barucci M. A., Emery J. P. et al. (2015) *The composition of “ultra-red” TNOs and centaurs*, *Icarus*, 252, 311–326.
- Dalle Ore C. M., Dalle Ore L. V., Roush T. L. et al. (2013) *A compositional interpretation of trans-neptunian objects taxonomies*, *Icarus*, 222, 307–322.
- Davies J. K., McFarland J., Bailey M. E. et al. (2008) in *The Solar System Beyond Neptune* (M. A. Barucci, H. Boehnhardt, D. P. Cruikshank, A. Morbidelli, and R. Dotson, eds.), pp. 11–23, Univ. of Arizona Press.
- Dawson R. I. and Murray-Clay R. (2012) *Neptune’s Wild Days: Constraints from the Eccentricity Distribution of the Classical Kuiper Belt*, *Astrophys. J.*, 750, 43.
- De Sanctis M. C., Capria M. T., Coradini A. et al. (2000) *Thermal Evolution of the Centaur Object 5145 Pholus*, *Astron. J.*, 120, 1571–1578.
- De Sousa R. R., Morbidelli A., Raymond S. N. et al. (2020) *Dynamical evidence for an early giant planet instability*, *Icarus*, 339, 113605.
- Deienno R., Morbidelli A., Gomes R. S. et al. (2017) *Constraining the Giant Planets’ Initial Configuration from Their Evolution: Implications for the Timing of the Planetary Instability*, *Astron. J.*, 153, 153.
- Dell’Oro A., Campo Bagatin A., Benavidez P. G. et al. (2013) *Statistics of encounters in the trans-Neptunian region*, *Astron. Astrophys.*, 558, A95.
- DeMeo F. E., Barucci M. A., Merlin F. et al. (2010) *A spectroscopic analysis of Jupiter-coupled object (52872) Okyrhoe, and TNOs (90482) Orcus and (73480) 2002 PN₃₄*, *Astron. Astrophys.*, 521, A35.
- DeMeo F. E., Binzel R. P., Slivan S. M. et al. (2009) *An extension of the Bus asteroid taxonomy into the near-infrared*, *Icarus*, 202, 160–180.
- Di Ruscio A., Fienga A., Durante D. et al. (2020) *Analysis of Cassini radio tracking data for the construction of INPOP19a: A new estimate of the Kuiper belt mass*, *Astron. Astrophys.*, 640, A7.
- Di Sisto R. P. and Brunini A. (2007) *The origin and distribution of the Centaur population*, *Icarus*, 190, 224–235.
- Di Sisto R. P., Brunini A., Dirani L. D. et al. (2005) *Hilda asteroids among Jupiter family comets*, *Icarus*, 174, 81–89.
- Di Sisto R. P., Fernández J. A., and Brunini A. (2009) *On the population, physical decay and orbital distribution of Jupiter family comets: Numerical simulations*, *Icarus*, 203, 140–154.
- Di Sisto R. P., Ramos X. S., and Gallardo T. (2019) *The dynamical evolution of escaped Jupiter Trojan asteroids, link to other minor body populations*, *Icarus*, 319, 828–839.
- Di Sisto R. P. and Rossignoli N. L. (2020) *Centaur and giant planet crossing populations: origin and distribution*, *Celestial Mechanics and Dynamical Astronomy*, 132, 36.
- Dohnanyi J. S. (1969) *Collisional Model of Asteroids and Their Debris*, *J. Geophys. Res.*, 74, 2531–2554.
- Dones L., Brassier R., Kaib N. et al. (2015) *Origin and Evolution of the Cometary Reservoirs*, *Space Sci. Rev.*, 197, 191–269.
- Dones L., Weissman P. R., Levison H. F. et al. (2004) in *Comets II* (M. C. Festou, H. U. Keller, and H. A. Weaver, eds.), p. 153, Univ. Arizona Press.
- Dotto E., Emery J. P., Barucci M. A. et al. (2008) in *The Solar System Beyond Neptune* (M. A. Barucci, H. Boehnhardt, D. P. Cruikshank, A. Morbidelli, and R. Dotson, eds.), pp. 383–395, Univ. of Arizona Press.
- Drahus M., Yang B., Lis D. C. et al. (2017) *New Limits to CO Outgassing in Centaurs*, *Mon. Not. R. Astron. Soc.*, 468, 2897–2909.
- Drozdovskaya M. N., Walsh C., van Dishoeck E. F. et al. (2016) *Cometary ices in forming protoplanetary disc midplanes*, *Mon. Not. R. Astron. Soc.*, 462, 977–993.
- Duncan M., Quinn T., and Tremaine S. (1987) *The Formation and Extent of the Solar System Comet Cloud*, *Astron. J.*, 94, 1330.
- Duncan M., Quinn T., and Tremaine S. (1988) *The Origin of Short-Period Comets*, *Astrophys. J. Lett.*, 328, L69.
- Duncan M. J. and Levison H. F. (1997) *A scattered comet disk and the origin of Jupiter family comets*, *Science*, 276, 1670–1672.
- Duncan M. J., Levison H. F., and Budd S. M. (1995) *The Dynamical Structure of the Kuiper Belt*, *Astron. J.*, 110, 3073.
- Edgeworth K. E. (1949) *The origin and evolution of the Solar System*, *Mon. Not. R. Astron. Soc.*, 109, 600–609.
- Elliot J. L., Kern S. D., Clancy K. B. et al. (2005) *The Deep Ecliptic Survey: A Search for Kuiper Belt Objects and Centaurs. II. Dynamical Classification, the Kuiper Belt Plane, and the Core Population*, *Astron. J.*, 129, 1117–1162.
- Emery J. P., Burr D. M., and Cruikshank D. P. (2011) *Near-infrared Spectroscopy of Trojan Asteroids: Evidence for Two Compositional Groups*, *Astron. J.*, 141, 25.
- Everhart E. (1972) *The Origin of Short-Period Comets*, *Astrophys. Lett.*, 10, 131.
- Fernández J. (2020) in *The Trans-Neptunian Solar System* (D. Pralnik, M. A. Barucci, and L. Young, eds.), pp. 1–22, Elsevier.
- Fernandez J. A. (1980) *On the existence of a comet belt beyond Neptune*, *Mon. Not. R. Astron. Soc.*, 192, 481–491.
- Fernández J. A., Gallardo T., and Brunini A. (2002) *Are There Many Inactive Jupiter-Family Comets among the Near-Earth Asteroid Population?*, *Icarus*, 159, 358–368.
- Fernández J. A., Helal M., and Gallardo T. (2018) *Dynamical evolution and end states of active and inactive Centaurs*, *Planet. Space Sci.*, 158, 6–15.
- Fernandez J. A. and Ip W. H. (1984) *Some dynamical aspects of the accretion of Uranus and Neptune: The exchange of orbital angular momentum with planetesimals*, *Icarus*, 58, 109–120.
- Fernández Y. R., Kelley M. S., Lamy P. L. et al. (2013) *Thermal properties, sizes, and size distribution of Jupiter-family cometary nuclei*, *Icarus*, 226, 1138–1170.
- Fernández-Valenzuela E. (2022) *Modeling Long-Term Photometric Data of Trans-Neptunian Objects and Centaurs*, *Frontiers in Astronomy and Space Sciences*, 9, 796004.
- Fernández-Valenzuela E., Pinilla-Alonso N., Stansberry J. et al. (2021) *Compositional Study of Trans-Neptunian Objects at $\lambda > 2.2 \mu\text{m}$* , *Planetary Sci. J.*, 2, 10.
- Festou M. C., Gunnarsson M., Rickman H. et al. (2001) *The Activity of Comet 29P/Schwassmann-Wachmann 1 Monitored through Its CO J=2→1 Radio Line*, *Icarus*, 150, 140–150.

- Fornasier S., Barucci M. A., de Bergh C. et al. (2009) *Visible spectroscopy of the new ESO large programme on trans-Neptunian objects and Centaurs: final results*, *Astron. Astrophys.*, 508, 457–465.
- Fornasier S., Lellouch E., Müller T. et al. (2013) *TNOs are Cool: A survey of the trans-Neptunian region. VIII. Combined Herschel PACS and SPIRE observations of nine bright targets at 70–500 μm* , *Astron. Astrophys.*, 555, A15.
- Fraser W., Brown M. E., Morbidelli A. et al. (2012) in *AAS/Division for Planetary Sciences Meeting Abstracts #44*, vol. 44 of *AAS/Division for Planetary Sciences Meeting Abstracts*, p. 502.03.
- Fraser W. C. (2009) *The Collisional Divot in the Kuiper Belt Size Distribution*, *Astrophys. J.*, 706, 119–129.
- Fraser W. C. and Brown M. E. (2012) *The Hubble Wide Field Camera 3 Test of Surfaces in the Outer Solar System: The Compositional Classes of the Kuiper Belt*, *Astrophys. J.*, 749, 33.
- Fraser W. C., Brown M. E., Morbidelli A. et al. (2014) *The Absolute Magnitude Distribution of Kuiper Belt Objects*, *Astrophys. J.*, 782, 100.
- Fraser W. C. and Kavelaars J. J. (2009) *The Size Distribution of Kuiper Belt Objects for $D \gtrsim 10$ km*, *Astron. J.*, 137, 72–82.
- Fraser W. C., Kavelaars J. J., Holman M. J. et al. (2008) *The Kuiper belt luminosity function from $m_R = 21$ to 26*, *Icarus*, 195, 827–843.
- Fuentes C. I., George M. R., and Holman M. J. (2009) *A Subaru Pencil-Beam Search for $m_R \sim 27$ Trans-Neptunian Bodies*, *Astrophys. J.*, 696, 91–95.
- Fulle M. (1992) *Dust from short-period comet P/Schwassmann-Wachmann 1 and replenishment of the interplanetary dust cloud*, *Nature*, 359, 42–44.
- Gil-Hutton R. and García-Migani E. (2016) *Comet candidates among quasi-Hilda objects*, *Astron. Astrophys.*, 590, A111.
- Gladman B. and Chan C. (2006) *Production of the Extended Scattered Disk by Rogue Planets*, *Astrophys. J. Lett.*, 643, L135–L138.
- Gladman B., Kavelaars J., Petit J. M. et al. (2009) *Discovery of the First Retrograde Transneptunian Object*, *Astrophys. J. Lett.*, 697, L91–L94.
- Gladman B., Kavelaars J. J., Nicholson P. D. et al. (1998) *Pencil-Beam Surveys for Faint Trans-Neptunian Objects*, *Astron. J.*, 116, 2042–2054.
- Gladman B., Kavelaars J. J., Petit J.-M. et al. (2001) *The Structure of the Kuiper Belt: Size Distribution and Radial Extent*, *Astron. J.*, 122, 1051–1066.
- Gladman B., Lawler S. M., Petit J. M. et al. (2012) *The Resonant Trans-Neptunian Populations*, *Astron. J.*, 144, 23.
- Gladman B., Marsden B. G., and Van Laerhoven C. (2008) in *The Solar System Beyond Neptune* (M. A. Barucci, H. Boehnhardt, D. P. Cruikshank, A. Morbidelli, and R. Dotson, eds.), pp. 43–57, Univ. Arizona Press.
- Gladman B. and Volk K. (2021) *Transneptunian space*, *Annual Review of Astronomy and Astrophysics*, 59, 203–246.
- Gomes R., Levison H. F., Tsiganis K. et al. (2005a) *Origin of the cataclysmic Late Heavy Bombardment period of the terrestrial planets*, *Nature*, 435, 466–469.
- Gomes R., Nesvorný D., Morbidelli A. et al. (2018) *Checking the compatibility of the cold Kuiper belt with a planetary instability migration model*, *Icarus*, 306, 319–327.
- Gomes R. S., Fernández J. A., Gallardo T. et al. (2008) in *The Solar System Beyond Neptune* (M. A. Barucci, H. Boehnhardt, D. P. Cruikshank, A. Morbidelli, and R. Dotson, eds.), pp. 259–273, Univ. Arizona Press.
- Gomes R. S., Gallardo T., Fernández J. A. et al. (2005b) *On The Origin of The High-Perihelion Scattered Disk: The Role of The Kozai Mechanism And Mean Motion Resonances*, *Celestial Mechanics and Dynamical Astronomy*, 91, 109–129.
- Gomes R. S., Morbidelli A., and Levison H. F. (2004) *Planetary migration in a planetesimal disk: why did Neptune stop at 30 AU?*, *Icarus*, 170, 492–507.
- Greenstreet S., Gladman B., and McKinnon W. B. (2015) *Impact and cratering rates onto Pluto*, *Icarus*, 258, 267–288.
- Greenstreet S., Gladman B., and McKinnon W. B. (2016) *Corrigendum to “Impact and Cratering Rates onto Pluto” [Icarus 258 (2015) 267–288]*, *Icarus*, 274, 366–367.
- Grundy W. M., Benecchi S. D., Rabinowitz D. L. et al. (2012) *Mutual events in the Cold Classical transneptunian binary system Sila and Nunam*, *Icarus*, 220, 74–83.
- Grundy W. M., Bird M. K., Britt D. T. et al. (2020) *Color, composition, and thermal environment of Kuiper Belt object (486958) Arrokoth*, *Science*, 367, aay3705.
- Grundy W. M., Noll K. S., Buie M. W. et al. (2019a) *The mutual orbit, mass, and density of transneptunian binary G'kún||'hòmdîmà (229762 2007 UK₁₂₆)*, *Icarus*, 334, 30–38.
- Grundy W. M., Noll K. S., Roe H. G. et al. (2019b) *Mutual orbit orientations of transneptunian binaries*, *Icarus*, 334, 62–78.
- Guilbert A., Alvarez-Candal A., Merlin F. et al. (2009) *ESO-Large Program on TNOs: Near-infrared spectroscopy with SINFONI*, *Icarus*, 201, 272–283.
- Guilbert-Lepoutre A. (2011) *A Thermal Evolution Model of Centaur 10199 Chariklo*, *Astron. J.*, 141, 103.
- Gulbis A. A. S., Elliot J. L., and Kane J. F. (2006) *The color of the Kuiper belt Core*, *Icarus*, 183, 168–178.
- Gunnarsson M., Bockelée-Morvan D., Biver N. et al. (2008) *Mapping the carbon monoxide coma of comet 29P/Schwassmann-Wachmann 1*, *Astron. Astrophys.*, 484, 537–546.
- Gunnarsson M., Bockelée-Morvan D., Winnberg A. et al. (2003) *Production and kinematics of CO in comet C/1995 O1 (Hale-Bopp) at large post-perihelion distances*, *Astron. Astrophys.*, 402, 383–393.
- Hahn J. M. and Malhotra R. (2005) *Neptune’s Migration into a Stirred-Up Kuiper Belt: A Detailed Comparison of Simulations to Observations*, *Astron. J.*, 130, 2392–2414.
- Hainaut O. R., Boehnhardt H., and Protopapa S. (2012) *Colours of minor bodies in the outer solar system. II. A statistical analysis revisited*, *Astron. Astrophys.*, 546, A115.
- Harrington Pinto O. and Womack M. (2019) in *EPSC-DPS Joint Meeting 2019*, vol. 2019, pp. EPSC–DPS2019–2064.
- Harsono D., Bruderer S., and van Dishoeck E. F. (2015) *Volatile snowlines in embedded disks around low-mass protostars*, *Astron. Astrophys.*, 582, A41.
- Hasegawa S., Marsset M., DeMeo F. E. et al. (2021) *Discovery of Two TNO-like Bodies in the Asteroid Belt*, *Astrophys. J. Lett.*, 916, L6.
- Hirabayashi M., Scheeres D. J., Chesley S. R. et al. (2016) *Fission and reconfiguration of bilobate comets as revealed by 67P/Churyumov-Gerasimenko*, *Nature*, 534, 352–355.
- Hofgartner J. D., Buratti B. J., Hayne P. O. et al. (2019) *Ongoing resurfacing of KBO Eris by volatile transport in local, collisional, sublimation atmosphere regime*, *Icarus*, 334, 52–61.
- Holler B. J., Grundy W. M., Buie M. W. et al. (2021) *The Eris/Dysnomia system I: The orbit of Dysnomia*, *Icarus*, 355, 114130.

- Horner J., Evans N. W., and Bailey M. E. (2004) *Simulations of the population of Centaurs - I. The bulk statistics*, *Mon. Not. R. Astron. Soc.*, 354, 798–810.
- Horner J., Evans N. W., Bailey M. E. et al. (2003) *The populations of comet-like bodies in the Solar system*, *Mon. Not. R. Astron. Soc.*, 343, 1057–1066.
- Horner J. and Lykawka P. S. (2010) *Planetary Trojans - the main source of short period comets?*, *International Journal of Astrobiology*, 9, 227–234.
- Hosek Jr. M. W., Blaauw R. C., Cooke W. J. et al. (2013) *Outburst Dust Production of Comet 29P/Schwassmann-Wachmann 1*, *Astron. J.*, 145, 122.
- Hsieh H. H., Novaković B., Walsh K. J. et al. (2020) *Potential Themis-family Asteroid Contribution to the Jupiter-family Comet Population*, *Astron. J.*, 159, 179.
- Hughes D. W. (1991) in *IAU Colloq. 116: Comets in the post-Halley era* (J. Newburn R. L., M. Neugebauer, and J. Rahe, eds.), vol. 167 of *Astrophysics and Space Science Library*, pp. 825–851.
- Hui M.-T. and Li J.-Y. (2018) *Is the Cometary Nucleus-extraction Technique Reliable?*, *PASP*, 130, 104501.
- Ivanova O., Agapitov O., Odstřil D. et al. (2019) *Dynamics of the CO⁺ coma of comet 29P/Schwassmann-Wachmann 1*, *Mon. Not. R. Astron. Soc.*, 486, 5614–5620.
- Ivanova O. V., Luk'yanyk I. V., Kiselev N. N. et al. (2016) *Photometric and spectroscopic analysis of Comet 29P/Schwassmann-Wachmann 1 activity*, *Planet. Space Sci.*, 121, 10–17.
- Ivanova O. V., Skorov Y. V., Korsun P. P. et al. (2011) *Observations of the long-lasting activity of the distant Comets 29P Schwassmann-Wachmann 1, C/2003 WT42 (LINEAR) and C/2002 VQ94 (LINEAR)*, *Icarus*, 211, 559–567.
- Izawa M. R. M., Applin D. M., Norman L. et al. (2014) *Reflectance spectroscopy (350–2500 nm) of solid-state polycyclic aromatic hydrocarbons (PAHs)*, *Icarus*, 237, 159–181.
- Izidoro A., Raymond S. N., Pierens A. et al. (2016) *The Asteroid Belt as a Relic from a Chaotic Early Solar System*, *Astrophys. J.*, 833, 40.
- Jewitt D. (2006) *Comet D/1819 WI (Blanpain): Not Dead Yet*, *Astron. J.*, 131, 2327–2331.
- Jewitt D. (2009) *The Active Centaurs*, *Astron. J.*, 137, 4296–4312.
- Jewitt D. (2015) *Color Systematics of Comets and Related Bodies*, *Astron. J.*, 150, 201.
- Jewitt D. (2021) *Systematics and Consequences of Comet Nucleus Outgassing Torques*, *Astron. J.*, 161, 261.
- Jewitt D., Hsieh H., and Agarwal J. (2015) in *Asteroids IV*, pp. 221–241, Univ. of Arizona Press.
- Jewitt D. and Luu J. (1993) *Discovery of the candidate Kuiper belt object 1992 QB₁*, *Nature*, 362, 730–732.
- Jewitt D., Luu J., and Trujillo C. (1998) *Large Kuiper Belt Objects: The Mauna Kea 8K CCD Survey*, *Astron. J.*, 115, 2125–2135.
- Jewitt D. C. (2004) in *Comets II* (M. C. Festou, H. U. Keller, and H. A. Weaver, eds.), pp. 659–676, Univ. Arizona Press.
- Jewitt D. C., Trujillo C. A., and Luu J. X. (2000) *Population and Size Distribution of Small Jovian Trojan Asteroids*, *Astron. J.*, 120, 1140–1147.
- Jones G. H., Knight M. M., Battams K. et al. (2018) *The Science of Sungrazers, Sunskirters, and Other Near-Sun Comets*, *Space Sci. Rev.*, 214, 20.
- Joss P. C. (1973) *On the Origin of Short-period Comets*, *Astron. Astrophys.*, 25, 271–273.
- Jutzi M. and Asphaug E. (2015) *The shape and structure of cometary nuclei as a result of low-velocity accretion*, *Science*, 348, 1355–1358.
- Jutzi M. and Benz W. (2017) *Formation of bi-lobed shapes by sub-catastrophic collisions. A late origin of comet 67P's structure*, *Astron. Astrophys.*, 597, A62.
- Kaib N. A. and Sheppard S. S. (2016) *Tracking Neptune's Migration History through High-perihelion Resonant Trans-Neptunian Objects*, *Astron. J.*, 152, 133.
- Kareta T., Sharkey B., Noonan J. et al. (2019) *Physical Characterization of the 2017 December Outburst of the Centaur 174P/Echeclus*, *Astron. J.*, 158, 255.
- Kareta T., Woodney L. M., Schambeau C. et al. (2021) *Contemporaneous Multiwavelength and Precovery Observations of the Active Centaur P/2019 LD2 (ATLAS)*, *Planetary Sci. J.*, 2, 48.
- Kavelaars J. J., Lawler S. M., Bannister M. T. et al. (2020) in *The Trans-Neptunian Solar System* (D. Prialnik, M. A. Barucci, and L. Young, eds.), pp. 61–77, Elsevier.
- Kavelaars J. J., Petit J.-M., Gladman B. et al. (2021) *OSSOS Finds an Exponential Cutoff in the Size Distribution of the Cold Classical Kuiper Belt*, *Astrophys. J. Lett.*, 920, L28.
- Kazimirschak-Polonskaya E. I. (1972) in *The Motion, Evolution of Orbits, and Origin of Comets* (G. A. Chebotarev, E. I. Kazimirschak-Polonskaya, and B. G. Marsden, eds.), vol. 45, pp. 373–397, Springer.
- Kelley M. S., Fernández Y. R., Licandro J. et al. (2013) *The persistent activity of Jupiter-family comets at 3–7 AU*, *Icarus*, 225, 475–494.
- Kelley M. S. P., Sharma K., Kumar H. et al. (2021) *Two Outbursts of Comet 29P/Schwassmann-Wachmann 1*, *The Astronomer's Telegram*, 14543, 1.
- Kenyon S. J., Bromley B. C., O'Brien D. P. et al. (2008) in *The Solar System Beyond Neptune* (M. A. Barucci, H. Boehnhardt, D. P. Cruikshank, A. Morbidelli, and R. Dotson, eds.), pp. 293–313, Univ. Arizona Press.
- Kozai Y. (1962) *Secular perturbations of asteroids with high inclination and eccentricity*, *Astron. J.*, 67, 591–598.
- Kresák L. (1972) *Jacobian integral as a classificational and evolutionary parameter of interplanetary bodies*, *Bulletin of the Astronomical Institutes of Czechoslovakia*, 23, 1–34.
- Kuiper G. P. (1951) in *50th Anniversary of the Yerkes Observatory and Half a Century of Progress in Astrophysics* (J. A. Hynek, ed.), pp. 357–424.
- Kulyk I., Korsun P., Rousselot P. et al. (2016) *P/2008 CL94 (Lemmon) and P/2011 S1 (Gibbs): comet-like activity at large heliocentric distances*, *Icarus*, 271, 314–325.
- Lacerda P., Fornasier S., Lellouch E. et al. (2014) *The Albedo-Color Diversity of Transneptunian Objects*, *Astrophys. J. Lett.*, 793, L2.
- Lamy P. L., Toth I., Fernandez Y. R. et al. (2004) in *Comets II* (M. C. Festou, H. U. Keller, and H. A. Weaver, eds.), pp. 223–264, Univ. Arizona Press.
- Lawler S. M., Kavelaars J. J., Alexandersen M. et al. (2018a) *OSSOS: X. How to use a Survey Simulator: Statistical Testing of Dynamical Models Against the Real Kuiper Belt*, *Frontiers in Astronomy and Space Sciences*, 5, 14.
- Lawler S. M., Pike R. E., Kaib N. et al. (2019) *OSSOS. XIII. Fossilized Resonant Dropouts Tentatively Confirm Neptune's Migration Was Rainy and Slow*, *Astron. J.*, 157, 253.
- Lawler S. M., Shankman C., Kavelaars J. J. et al. (2018b) *OSSOS. VIII. The Transition between Two Size Distribution Slopes in the Scattering Disk*, *Astron. J.*, 155, 197.

- Levison H. F. (1996) in *Completing the Inventory of the Solar System* (T. Rettig and J. M. Hahn, eds.), vol. 107 of *Astronomical Society of the Pacific Conference Series*, pp. 173–191.
- Levison H. F., Bottke W. F., Gounelle M. et al. (2009) *Contamination of the asteroid belt by primordial trans-Neptunian objects*, *Nature*, 460, 364–366.
- Levison H. F. and Duncan M. J. (1994) *The Long-Term Dynamical Behavior of Short-Period Comets*, *Icarus*, 108, 18–36.
- Levison H. F. and Duncan M. J. (1997) *From the Kuiper Belt to Jupiter-Family Comets: The Spatial Distribution of Ecliptic Comets*, *Icarus*, 127, 13–32.
- Levison H. F., Duncan M. J., Dones L. et al. (2006a) *The scattered disk as a source of Halley-type comets*, *Icarus*, 184, 619–633.
- Levison H. F., Duncan M. J., Zahnle K. et al. (2000) *Note: Planetary Impact Rates from Ecliptic Comets*, *Icarus*, 143, 415–420.
- Levison H. F., Morbidelli A., Tsiganis K. et al. (2011) *Late Orbital Instabilities in the Outer Planets Induced by Interaction with a Self-gravitating Planetesimal Disk*, *Astron. J.*, 142, 152.
- Levison H. F., Morbidelli A., Van Laerhoven C. et al. (2008) *Origin of the structure of the Kuiper belt during a dynamical instability in the orbits of Uranus and Neptune*, *Icarus*, 196, 258–273.
- Levison H. F. and Stern S. A. (2001) *On the Size Dependence of the Inclination Distribution of the Main Kuiper Belt*, *Astron. J.*, 121, 1730–1735.
- Levison H. F., Terrell D., Wiegert P. A. et al. (2006b) *On the origin of the unusual orbit of Comet 2P/Encke*, *Icarus*, 182, 161–168.
- Li R., Youdin A. N., and Simon J. B. (2019) *Demographics of Planetesimals Formed by the Streaming Instability*, *Astrophys. J.*, 885, 69.
- Licandro J., de León J., Moreno F. et al. (2021) *Activity of the Jupiter co-orbital comet P/2019 LD₂ (ATLAS) observed with OSIRIS at the 10.4 m GTC*, *Astron. Astrophys.*, 650, A79.
- Lilly E., Hsieh H., Bauer J. et al. (2021) *No Activity among 13 Centaurs Discovered in the Pan-STARRS1 Detection Database*, *Planetary Sci. J.*, 2, 155.
- Lisse C., Bauer J., Cruikshank D. et al. (2020) *Spitzer’s Solar System studies of comets, centaurs and Kuiper belt objects*, *Nature Astronomy*, 4, 930–939.
- Lisse C. M., Young L. A., Cruikshank D. P. et al. (2021) *On the origin & thermal stability of Arrokoth’s and Pluto’s ices*, *Icarus*, 356, 114072.
- Lithwick Y. (2014) *After Runaway: The Trans-Hill Stage of Planetesimal Growth*, *Astrophys. J.*, 780, 22.
- LSST Science Collaboration, Abell P. A., Allison J. et al. (2009) *LSST Science Book, Version 2.0*, *arXiv e-prints*, arXiv:0912.0201.
- Luu J., Marsden B. G., Jewitt D. et al. (1997) *A new dynamical class of object in the outer Solar System*, *Nature*, 387, 573–575.
- Luu J. X. and Jewitt D. C. (1990) *Cometary Activity in 2060 Chiron*, *Astron. J.*, 100, 913–932.
- Lykawka P. S. and Mukai T. (2007) *Dynamical classification of trans-neptunian objects: Probing their origin, evolution, and interrelation*, *Icarus*, 189, 213–232.
- Lykawka P. S. and Mukai T. (2008) *An Outer Planet Beyond Pluto and the Origin of the Trans-Neptunian Belt Architecture*, *Astron. J.*, 135, 1161–1200.
- Lyra W. and Umurhan O. M. (2019) *The Initial Conditions for Planet Formation: Turbulence Driven by Hydrodynamical Instabilities in Disks around Young Stars*, *PASP*, 131, 072001.
- Mahjoub A., Brown M. E., Poston M. J. et al. (2021) *Effect of H₂S on the Near-infrared Spectrum of Irradiation Residue and Applications to the Kuiper Belt Object (486958) Arrokoth*, *Astrophys. J. Lett.*, 914, L31.
- Malhotra R. (1993) *The origin of Pluto’s peculiar orbit*, *Nature*, 365, 819–821.
- Malhotra R. (1995) *The Origin of Pluto’s Orbit: Implications for the Solar System Beyond Neptune*, *Astron. J.*, 110, 420–429.
- Malhotra R. (2019) *Resonant Kuiper belt objects: a review*, *Geoscience Letters*, 6, 12.
- Marboeuf U., Thiabaud A., Alibert Y. et al. (2014) *From stellar nebula to planetesimals*, *Astron. Astrophys.*, 570, A35.
- Marsset M., Fraser W. C., Pike R. E. et al. (2019) *Col-OSSOS: Color and Inclination Are Correlated throughout the Kuiper Belt*, *Astron. J.*, 157, 94.
- Martin A. C., Emery J. P., and Loeffler M. J. (2022) *Spectral effects of regolith porosity in the mid-IR - Forsteritic olivine*, *Icarus*, 378, 114921.
- Matthews B. C., Krivov A. V., Wyatt M. C. et al. (2014) in *Protostars and Planets VI* (H. Beuther, R. S. Klessen, C. P. Dullemond, and T. Henning, eds.), pp. 521–544.
- McKinnon W. B., Richardson D. C., Marohnic J. C. et al. (2020) *The solar nebula origin of (486958) Arrokoth, a primordial contact binary in the Kuiper Belt*, *Science*, 367, aay6620.
- Meech K. J., Hainaut O. R., and Marsden B. G. (2004) *Comet nucleus size distributions from HST and Keck telescopes*, *Icarus*, 170, 463–491.
- Merlin F., Barucci M. A., de Bergh C. et al. (2010) *Chemical and physical properties of the variegated Pluto and Charon surfaces*, *Icarus*, 210, 930–943.
- Mojzsis S. J., Brasser R., Kelly N. M. et al. (2019) *Onset of Giant Planet Migration before 4480 Million Years Ago*, *Astrophys. J.*, 881, 44.
- Morbidelli A. (1997) *Chaotic Diffusion and the Origin of Comets from the 2/3 Resonance in the Kuiper Belt*, *Icarus*, 127, 1–12.
- Morbidelli A., Bottke W. F., Nesvorný D. et al. (2009a) *Asteroids were born big*, *Icarus*, 204, 558–573.
- Morbidelli A., Brasser R., Gomes R. et al. (2010) *Evidence from the Asteroid Belt for a Violent Past Evolution of Jupiter’s Orbit*, *Astron. J.*, 140, 1391–1401.
- Morbidelli A., Levison H. F., Bottke W. F. et al. (2009b) *Considerations on the magnitude distributions of the Kuiper belt and of the Jupiter Trojans*, *Icarus*, 202, 310–315.
- Morbidelli A. and Nesvorný D. (2020) in *The Trans-Neptunian Solar System* (D. Prialnik, M. A. Barucci, and L. Young, eds.), pp. 25–59, Elsevier.
- Morbidelli A. and Rickman H. (2015) *Comets as collisional fragments of a primordial planetesimal disk*, *Astron. Astrophys.*, 583, A43.
- Mumma M. J. and Charnley S. B. (2011) *The Chemical Composition of Comets—Emerging Taxonomies and Natal Heritage*, *Annu. Rev. Astron. Astrophys.*, 49, 471–524.
- Napier K. J., Gerdes D. W., Lin H. W. et al. (2021) *No Evidence for Orbital Clustering in the Extreme Trans-Neptunian Objects*, *Planetary Sci. J.*, 2, 59.
- Nesvorný D. (2011) *Young Solar System’s Fifth Giant Planet?*, *Astrophys. J. Lett.*, 742, L22.
- Nesvorný D. (2015) *Evidence for Slow Migration of Neptune from the Inclination Distribution of Kuiper Belt Objects*, *Astron. J.*, 150, 73.
- Nesvorný D. (2018) *Dynamical Evolution of the Early Solar System*, *Annu. Rev. Astron. Astrophys.*, 56, 137–174.
- Nesvorný D. (2020) *Influence of Neptune’s Migration Parameters*

- on the Inclination Distribution of Kuiper Belt Objects (KBOs), *Research Notes of the American Astronomical Society*, 4, 212.
- Nesvorný D. (2021) *Eccentric Early Migration of Neptune*, *Astrophys. J. Lett.*, 908, L47.
- Nesvorný D., Li R., Youdin A. N. et al. (2019a) *Trans-Neptunian binaries as evidence for planetesimal formation by the streaming instability*, *Nature Astronomy*, 3, 808–812.
- Nesvorný D. and Morbidelli A. (2012) *Statistical Study of the Early Solar System's Instability with Four, Five, and Six Giant Planets*, *Astron. J.*, 144, 117.
- Nesvorný D., Roig F., and Ferraz-Mello S. (2000) *Close Approaches of Trans-Neptunian Objects to Pluto Have Left Observable Signatures on Their Orbital Distribution*, *Astron. J.*, 119, 953–969.
- Nesvorný D., Roig F. V., and Deienno R. (2021) *The Role of Early Giant-planet Instability in Terrestrial Planet Formation*, *Astron. J.*, 161, 50.
- Nesvorný D. and Vokrouhlický D. (2016) *Neptune's Orbital Migration Was Grainy, Not Smooth*, *Astrophys. J.*, 825, 94.
- Nesvorný D. and Vokrouhlický D. (2019) *Binary survival in the outer solar system*, *Icarus*, 331, 49–61.
- Nesvorný D., Vokrouhlický D., Alexandersen M. et al. (2020) *OS-SOS XX: The Meaning of Kuiper Belt Colors*, *Astron. J.*, 160, 46.
- Nesvorný D., Vokrouhlický D., Bottke W. F. et al. (2011) *Observed Binary Fraction Sets Limits on the Extent of Collisional Grinding in the Kuiper Belt*, *Astron. J.*, 141, 159.
- Nesvorný D., Vokrouhlický D., and Deienno R. (2014) *Capture of Irregular Satellites at Jupiter*, *Astrophys. J.*, 784, 22.
- Nesvorný D., Vokrouhlický D., Dones L. et al. (2017) *Origin and Evolution of Short-period Comets*, *Astrophys. J.*, 845, 27.
- Nesvorný D., Vokrouhlický D., and Morbidelli A. (2013) *Capture of Trojans by Jumping Jupiter*, *Astrophys. J.*, 768, 45.
- Nesvorný D., Vokrouhlický D., and Roig F. (2016) *The Orbital Distribution of Trans-Neptunian Objects Beyond 50 au*, *Astrophys. J. Lett.*, 827, L35.
- Nesvorný D., Vokrouhlický D., Stern A. S. et al. (2019b) *OSSOS. XIX. Testing Early Solar System Dynamical Models Using OS-SOS Centaur Detections*, *Astron. J.*, 158, 132.
- Noll K., Grundy W. M., Nesvorný D. et al. (2020) in *The Trans-Neptunian Solar System* (D. Prrialnik, M. A. Barucci, and L. Young, eds.), pp. 201–224, Elsevier.
- Noll K. S., Grundy W. M., Stephens D. C. et al. (2008) *Evidence for two populations of classical transneptunian objects: The strong inclination dependence of classical binaries*, *Icarus*, 194, 758–768.
- Noonan J. W., Harris W. M., Bromley S. et al. (2021) *FUV Observations of the Inner Coma of 46P/Wirtanen*, *Planetary Sci. J.*, 2, 8.
- Öberg K. I., Murray-Clay R., and Bergin E. A. (2011) *The Effects of Snowlines on C/O in Planetary Atmospheres*, *Astrophys. J. Lett.*, 743, L16.
- O'Brien D. P. and Greenberg R. (2003) *Steady-state size distributions for collisional populations: analytical solution with size-dependent strength*, *Icarus*, 164, 334–345.
- Ohtsuka K., Ito T., Yoshikawa M. et al. (2008) *Quasi-Hilda comet 147P/Kushida-Muramatsu. Another long temporary satellite capture by Jupiter*, *Astron. Astrophys.*, 489, 1355–1362.
- Oort J. H. (1950) *The structure of the cloud of comets surrounding the Solar System and a hypothesis concerning its origin*, *Bull. Astron. Inst. Netherlands*, 11, 91–110.
- Ootsubo T., Kawakita H., Hamada S. et al. (2012) *AKARI Near-infrared Spectroscopic Survey for CO₂ in 18 Comets*, *Astrophys. J.*, 752, 15.
- Paganini L., Mumma M. J., Boehnhardt H. et al. (2013) *Ground-Based Infrared Detections of CO in the Centaur-comet 29P/Schwassmann-Wachmann 1 at 6.26 AU from the Sun*, *Astrophys. J.*, 766, 100.
- Parker A., Pinilla-Alonso N., Santos-Sanz P. et al. (2016) *Physical Characterization of TNOs with the James Webb Space Telescope*, *PASP*, 128, 018010.
- Parker A. H. (2021) in *The Pluto System After New Horizons* (S. A. Stern, J. M. Moore, W. M. Grundy, L. A. Young, and R. P. Binzel, eds.), pp. 545–568, Univ. Arizona Press.
- Parker A. H. and Kavelaars J. J. (2010) *Destruction of Binary Minor Planets During Neptune Scattering*, *Astrophys. J. Lett.*, 722, L204–L208.
- Peixinho N., Delsanti A., and Doressoundiram A. (2015) *Reanalyzing the visible colors of Centaurs and KBOs: what is there and what we might be missing*, *Astron. Astrophys.*, 577, A35.
- Peixinho N., Delsanti A., Guilbert-Lepoutre A. et al. (2012) *The bimodal colors of Centaurs and small Kuiper belt objects*, *Astron. Astrophys.*, 546, A86.
- Peixinho N., Thirouin A., Tegler S. C. et al. (2020) in *The Trans-Neptunian Solar System* (D. Prrialnik, M. A. Barucci, and L. Young, eds.), pp. 307–329, Elsevier.
- Petit J. M., Kavelaars J. J., Gladman B. J. et al. (2011) *The Canada-France Ecliptic Plane Survey—Full Data Release: The Orbital Structure of the Kuiper Belt*, *Astron. J.*, 142, 131.
- Pike R. E., Fraser W. C., Schwamb M. E. et al. (2017) *Col-OSSOS: z-Band Photometry Reveals Three Distinct TNO Surface Types*, *Astron. J.*, 154, 101.
- Presler-Marshall B., Schleicher D. G., Knight M. M. et al. (2020) in *AAS/Division for Planetary Sciences Meeting Abstracts*, vol. 52 of *AAS/Division for Planetary Sciences Meeting Abstracts*, p. 212.06.
- Prrialnik D., Brosch N., and Ianovici D. (1995) *Modelling the activity of 2060 Chiron*, *Mon. Not. R. Astron. Soc.*, 276, 1148–1154.
- Prrialnik D., Sarid G., Rosenberg E. D. et al. (2008) *Thermal and Chemical Evolution of Comet Nuclei and Kuiper Belt Objects*, *Space Sci. Rev.*, 138, 147–164.
- Protopapa S., Kelley M. S. P., Yang B. et al. (2018) *Icy Grains from the Nucleus of Comet C/2013 US₁₀ (Catalina)*, *Astrophys. J. Lett.*, 862, L16.
- Quarles B. and Kaib N. (2019) *Instabilities in the Early Solar System Due to a Self-gravitating Disk*, *Astron. J.*, 157, 67.
- Raymond S. N., Armitage P. J., Veras D. et al. (2018) *Implications of the interstellar object II/Oumuamua for planetary dynamics and planetesimal formation*, *Mon. Not. R. Astron. Soc.*, 476, 3031–3038.
- Raymond S. N. and Nesvorný D. (2022) in *Vesta and Ceres. Insights from the Dawn Mission for the Origin of the Solar System* (S. Marchi, C. A. Raymond, and C. T. Russell, eds.), pp. 227–249, Cambridge University Press.
- Rickman H., Fernandez J. A., and Gustafson B. A. S. (1990) *Formation of stable dust mantles on short-period comet nuclei*, *Astron. Astrophys.*, 237, 524–535.
- Rickman H., Kamél L., Froeschlé C. et al. (1991) *Nongravitational effects and the aging of periodic comets*, *Astron. J.*, 102, 1446–1463.
- Robbins S. J. and Singer K. N. (2021) *Pluto and Charon Impact Crater Populations: Reconciling Different Results*, *Planetary Sci. J.*, 2, 192.

- Robinson J. E., Fraser W. C., Fitzsimmons A. et al. (2020) *Investigating gravitational collapse of a pebble cloud to form transneptunian binaries*, *Astron. Astrophys.*, 643, A55.
- Romon-Martin J., Delahodde C., Barucci M. A. et al. (2003) *Photometric and spectroscopic observations of (2060) Chiron at the ESO Very Large Telescope*, *Astron. Astrophys.*, 400, 369–373.
- Roush T. L. and Dalton J. B. (2004) *Reflectance spectra of hydrated Titan tholins at cryogenic temperatures and implications for compositional interpretation of red objects in the outer Solar System*, *Icarus*, 168, 158–162.
- Rousselot P. (2008) *174P/Echeclus: a strange case of outburst*, *Astron. Astrophys.*, 480, 543–550.
- Rousselot P., Korsun P. P., Kulyk I. et al. (2016) *A long-term follow up of 174P/Echeclus*, *Mon. Not. R. Astron. Soc.*, 462, S432–S442.
- Rowan-Robinson M. (2022) *A search for Planet 9 in the IRAS data*, *Mon. Not. R. Astron. Soc.*, 510, 3716–3726.
- Safrit T. K., Steckloff J. K., Bosh A. S. et al. (2021) *The Formation of Bilobate Comet Shapes through Sublimative Torques*, *Planetary Sci. J.*, 2, 14.
- Saki M., Gibb E. L., Bonev B. P. et al. (2020) *Carbonyl Sulfide (OCS): Detections in Comets C/2002 T7 (LINEAR), C/2015 ER61 (PanSTARRS), and 21P/Giacobini-Zinner and Stringent Upper Limits in 46P/Wirtanen*, *Astron. J.*, 160, 184.
- Sarid G., Volk K., Steckloff J. K. et al. (2019) *29P/Schwassmann-Wachmann 1, A Centaur in the Gateway to the Jupiter-family Comets*, *Astrophys. J. Lett.*, 883, L25.
- Schaller E. L. and Brown M. E. (2007) *Volatile Loss and Retention on Kuiper Belt Objects*, *Astrophys. J. Lett.*, 659, L61–L64.
- Schambeau C. A., Fernández Y. R., Samarasinha N. H. et al. (2017) *Analysis of R-band observations of an outburst of Comet 29P/Schwassmann-Wachmann 1 to place constraints on the nucleus' rotation state*, *Icarus*, 284, 359–371.
- Schambeau C. A., Fernández Y. R., Samarasinha N. H. et al. (2021) *Characterization of Thermal-infrared Dust Emission and Refinements to the Nucleus Properties of Centaur 29P/Schwassmann-Wachmann 1*, *Planetary Sci. J.*, 2, 126.
- Schambeau C. A., Fernández Y. R., Samarasinha N. H. et al. (2019) *Analysis of HST WFPC2 Observations of Centaur 29P/Schwassmann-Wachmann 1 while in Outburst to Place Constraints on the Nucleus' Rotation State*, *Astron. J.*, 158, 259.
- Schlichting H. E., Ofek E. O., Sari R. et al. (2012) *Measuring the Abundance of Sub-kilometer-sized Kuiper Belt Objects Using Stellar Occultations*, *Astrophys. J.*, 761, 150.
- Schwamb M. E., Fraser W. C., Bannister M. T. et al. (2019) *ColOSSOS: The Colors of the Outer Solar System Origins Survey*, *Astrophys. J. Suppl.*, 243, 12.
- Schwartz S. R., Michel P., Jutzi M. et al. (2018) *Catastrophic disruptions as the origin of bilobate comets*, *Nature Astronomy*, 2, 379–382.
- Secull T., Fraser W. C., and Puzia T. H. (2021) *Near-UV Reddening Observed in the Reflectance Spectrum of High-inclination Centaur 2012 DR₃₀*, *Planetary Sci. J.*, 2, 239.
- Secull T., Fraser W. C., Puzia T. H. et al. (2018) *2004 EW₉₅: A Phyllosilicate-bearing Carbonaceous Asteroid in the Kuiper Belt*, *Astrophys. J. Lett.*, 855, L26.
- Secull T., Fraser W. C., Puzia T. H. et al. (2019) *174P/Echeclus and Its Blue Coma Observed Post-outburst*, *Astron. J.*, 157, 88.
- Sedgwick C. and Serjeant S. (2022) *Searching for giant planets in the outer Solar System with far-infrared all-sky surveys*, *Mon. Not. R. Astron. Soc.*, 515, 4828–4837.
- Seligman D. Z., Kratter K. M., Levine W. G. et al. (2021) *A Sublime Opportunity: The Dynamics of Transitioning Cometary Bodies and the Feasibility of In Situ Observations of the Evolution of Their Activity*, *Planetary Sci. J.*, 2, 234.
- Senay M. C. and Jewitt D. (1994) *Coma formation driven by carbon monoxide release from comet Schwassmann-Wachmann 1*, *Nature*, 371, 229–231.
- Shankman C., Gladman B. J., Kaib N. et al. (2013) *A Possible Divot in the Size Distribution of the Kuiper Belt's Scattering Objects*, *Astrophys. J. Lett.*, 764, L2.
- Shankman C., Kavelaars J. J., Bannister M. T. et al. (2017) *OS-SOS. VI. Striking Biases in the Detection of Large Semimajor Axis Trans-Neptunian Objects*, *Astron. J.*, 154, 50.
- Shannon A., Doressoundiram A., Roques F. et al. (2021) *Understanding the trans-Neptunian Solar system: Reconciling the results of serendipitous stellar occultations and the inferences from the cratering record*, *arXiv e-prints*, arXiv:2111.00391.
- Sheppard S. S. and Jewitt D. (2004) *Extreme Kuiper Belt Object 2001 QG₂₉₈ and the Fraction of Contact Binaries*, *Astron. J.*, 127, 3023–3033.
- Sheppard S. S. and Trujillo C. A. (2010) *The Size Distribution of the Neptune Trojans and the Missing Intermediate-sized Planetesimals*, *Astrophys. J. Lett.*, 723, L233–L237.
- Sheppard S. S., Trujillo C. A., Tholen D. J. et al. (2019) *A New High Perihelion Trans-Plutonian Inner Oort Cloud Object: 2015 TG387*, *Astron. J.*, 157, 139.
- Showalter M. R., Benecchi S. D., Buie M. W. et al. (2021) *A statistical review of light curves and the prevalence of contact binaries in the Kuiper Belt*, *Icarus*, 356, 114098.
- Sickafoose A. A., Bosh A. S., Emery J. P. et al. (2020) *Characterization of material around the centaur (2060) Chiron from a visible and near-infrared stellar occultation in 2011*, *Mon. Not. R. Astron. Soc.*, 491, 3643–3654.
- Singer K. N., McKinnon W. B., Gladman B. et al. (2019) *Impact craters on Pluto and Charon indicate a deficit of small Kuiper belt objects*, *Science*, 363, 955–959.
- Singer K. N., Stern S. A., Elliott J. et al. (2021) *A new spacecraft mission concept combining the first exploration of the Centaurs and an astrophysical space telescope for the outer solar system*, *Planet. Space Sci.*, 205, 105290.
- Smullen R. A. and Volk K. (2020) *Machine learning classification of Kuiper belt populations*, *Mon. Not. R. Astron. Soc.*, 497, 1391–1403.
- Snodgrass C., Fitzsimmons A., Lowry S. C. et al. (2011) *The size distribution of Jupiter Family comet nuclei*, *Mon. Not. R. Astron. Soc.*, 414, 458–469.
- Steckloff J. K., Sarid G., Volk K. et al. (2020) *P/2019 LD2 (ATLAS): An Active Centaur in Imminent Transition to the Jupiter Family*, *Astrophys. J. Lett.*, 904, L20.
- Stern S. A., Weaver H. A., Spencer J. R. et al. (2019) *Initial results from the New Horizons exploration of 2014 MU₆₉, a small Kuiper Belt object*, *Science*, 364, aaw9771.
- Tancredi G., Lindgren M., and Rickman H. (1990) *Temporary satellite capture and orbital evolution of Comet P/Helin-Roman-Crockett*, *Astron. Astrophys.*, 239, 375–380.
- Tegler S., Consolmagno G., and Romanishin W. (2006) *Comet 174P/Echeclus*, *IAU Circ.*, 8701, 1.
- Tegler S. C. and Romanishin W. (1998) *Two distinct populations of Kuiper-belt objects*, *Nature*, 392, 49–51.
- Tegler S. C., Romanishin W., Consolmagno G. J. et al. (2016) *Two Color Populations of Kuiper Belt and Centaur Objects and the*

- Smaller Orbital Inclinations of Red Centaur Objects*, *Astron. J.*, 152, 210.
- Thirouin A. and Sheppard S. S. (2018) *The Plutino Population: An Abundance of Contact Binaries*, *Astron. J.*, 155, 248.
- Thirouin A. and Sheppard S. S. (2019) *Light Curves and Rotational Properties of the Pristine Cold Classical Kuiper Belt Objects*, *Astron. J.*, 157, 228.
- Thirouin A. and Sheppard S. S. (2022) *Lightcurves and Rotations of Trans-Neptunian Objects in the 2:1 Mean Motion Resonance with Neptune*, *Planetary Sci. J.*, 3, 178.
- Thompson W. R., Murray B. G. J. P. T., Khare B. N. et al. (1987) *Coloration and darkening of methane clathrate and other ices by charged particle irradiation: Applications to the outer solar system*, *J. Geophys. Res.*, 92, 14933–14947.
- Tiscareno M. S. and Malhotra R. (2003) *The Dynamics of Known Centaurs*, *Astron. J.*, 126, 3122–3131.
- Tiscareno M. S. and Malhotra R. (2009) *Chaotic Diffusion of Resonant Kuiper Belt Objects*, *Astron. J.*, 138, 827–837.
- Toth I. (2006) *The quasi-Hilda subgroup of ecliptic comets - an update*, *Astron. Astrophys.*, 448, 1191–1196.
- Trigo-Rodríguez J. M., García-Hernández D. A., Sánchez A. et al. (2010) *Outburst activity in comets - II. A multiband photometric monitoring of comet 29P/Schwassmann-Wachmann 1*, *Mon. Not. R. Astron. Soc.*, 409, 1682–1690.
- Trujillo C. A., Brown M. E., Barkume K. M. et al. (2007) *The Surface of 2003 EL₆₁ in the Near-Infrared*, *Astrophys. J.*, 655, 1172–1178.
- Trujillo C. A., Jewitt D. C., and Luu J. X. (2001) *Properties of the Trans-Neptunian Belt: Statistics from the Canada-France-Hawaii Telescope Survey*, *Astron. J.*, 122, 457–473.
- Trujillo C. A. and Sheppard S. S. (2014) *A Sedna-like body with a perihelion of 80 astronomical units*, *Nature*, 507, 471–474.
- Trujillo C. A., Sheppard S. S., and Schaller E. L. (2011) *A Photometric System for Detection of Water and Methane Ices on Kuiper Belt Objects*, *Astrophys. J.*, 730, 105.
- Tsiganis K., Gomes R., Morbidelli A. et al. (2005) *Origin of the orbital architecture of the giant planets of the Solar System*, *Nature*, 435, 459–461.
- Valsecchi G. B., Morbidelli A., Gonczi R. et al. (1995) *The Dynamics of Objects in Orbits Resembling That of P/Encke*, *Icarus*, 118, 169–180.
- van der Wiel M. H. D., Naylor D. A., Kamp I. et al. (2014) *Signatures of warm carbon monoxide in protoplanetary discs observed with Herschel SPIRE*, *Mon. Not. R. Astron. Soc.*, 444, 3911–3925.
- Villanueva G. L., Smith M. D., Protopapa S. et al. (2018) *Planetary Spectrum Generator: An accurate online radiative transfer suite for atmospheres, comets, small bodies and exoplanets*, *J. Quant. Spec. Radiat. Transf.*, 217, 86–104.
- Vokrouhlický D., Bottke W. F., and Nesvorný D. (2016) *Capture of Trans-Neptunian Planetesimals in the Main Asteroid Belt*, *Astron. J.*, 152, 39.
- Vokrouhlický D., Nesvorný D., and Dones L. (2019) *Origin and Evolution of Long-period Comets*, *Astron. J.*, 157, 181.
- Volk K. and Malhotra R. (2008) *The Scattered Disk as the Source of the Jupiter Family Comets*, *Astrophys. J.*, 687, 714–725.
- Volk K. and Malhotra R. (2013) *Do Centaurs preserve their source inclinations?*, *Icarus*, 224, 66–73.
- Volk K. and Malhotra R. (2019) *Not a Simple Relationship between Neptune’s Migration Speed and Kuiper Belt Inclination Excitation*, *Astron. J.*, 158, 64.
- Volk K., Murray-Clay R., Gladman B. et al. (2016) *OSSOS III—Resonant Trans-Neptunian Populations: Constraints from the first quarter of the Outer Solar System Origins Survey*, *Astron. J.*, 152, 23.
- Wang J. H. and Brasser R. (2014) *An Oort Cloud origin of the Halley-type comets*, *Astron. Astrophys.*, 563, A122.
- Weissman P. R. (1996) in *Completing the Inventory of the Solar System* (T. Rettig and J. M. Hahn, eds.), vol. 107 of *Astronomical Society of the Pacific Conference Series*, pp. 265–288.
- Whitney C. (1955) *Comet outbursts*, *Astrophys. J.*, 122, 190–195.
- Wiegert P. and Tremaine S. (1999) *The Evolution of Long-Period Comets*, *Icarus*, 137, 84–121.
- Wierzchos K. and Womack M. (2020) *CO Gas and Dust Outbursts from Centaur 29P/Schwassmann-Wachmann*, *Astron. J.*, 159, 136.
- Wierzchos K., Womack M., and Sarid G. (2017) *Carbon Monoxide in the Distantly Active Centaur (60558) 174P/Echeclus at 6 au*, *Astron. J.*, 153, 230.
- Womack M., Festou M. C., and Stern S. A. (1997) *The Heliocentric Evolution of Key Species in the Distantly-Active Comet C/1995 O1 (Hale-Bopp)*, *Astron. J.*, 114, 2789.
- Womack M., Sarid G., and Wierzchos K. (2017) *CO in Distantly Active Comets*, *PASP*, 129, 031001.
- Womack M. and Stern S. A. (1999) *The Detection of Carbon Monoxide Gas Emission in (2060) Chiron*, *Solar System Research*, 33, 187.
- Wong E. W., Brasser R., and Werner S. C. (2021) *Early impact chronology of the icy regular satellites of the outer solar system*, *Icarus*, 358, 114184.
- Wong I. and Brown M. E. (2015) *The Color-Magnitude Distribution of Small Jupiter Trojans*, *Astron. J.*, 150, 174.
- Wong I. and Brown M. E. (2016) *A Hypothesis for the Color Bimodality of Jupiter Trojans*, *Astron. J.*, 152, 90.
- Wong I. and Brown M. E. (2017) *The Bimodal Color Distribution of Small Kuiper Belt Objects*, *Astron. J.*, 153, 145.
- Yang B., Jewitt D., and Bus S. J. (2009) *Comet 17P/Holmes in Outburst: The Near Infrared Spectrum*, *Astron. J.*, 137, 4538–4546.
- Yang B., Jewitt D., Zhao Y. et al. (2021) *Discovery of Carbon Monoxide in Distant Comet C/2017 K2 (PANSTARRS)*, *Astrophys. J. Lett.*, 914, L17.
- Yoshida F., Terai T., Ito T. et al. (2019) *A comparative study of size frequency distributions of Jupiter Trojans, Hildas and main belt asteroids: A clue to planet migration history*, *Planet. Space Sci.*, 169, 78–85.
- Yoshida F., Terai T., Ito T. et al. (2020) *A comparative study of size frequency distributions of Jupiter Trojans, Hildas and main belt asteroids: A clue to planet migration history (corrigendum)*, *Planet. Space Sci.*, 190, 104977.
- Youdin A. N. and Goodman J. (2005) *Streaming Instabilities in Protoplanetary Disks*, *Astrophys. J.*, 620, 459–469.
- Zheng W., Jewitt D., and Kaiser R. I. (2009) *On the State of Water Ice on Saturn’s Moon Titan and Implications to Icy Bodies in the Outer Solar System*, *Journal of Physical Chemistry A*, 113, 11174–11181.